

國立交通大學

電信工程學系

碩士論文

在信號源不足環境下手機的定位和軌跡追蹤演算法

Wireless Location Tracking Algorithm  
for Environments with Insufficient  
Signal Sources

研究生：林育群

指導教授：方凱田

中華民國九十六年六月

在信號源不足環境下手機的定位和軌跡追蹤演算法

Wireless Location Tracking Algorithm for Environments  
with Insufficient Signal Sources

研究生：林育群

Student : Yu-Chun Lin

指導教授：方凱田

Advisor : Kai-Ten Feng



A Thesis

Submitted to Department of Communication Engineering  
College of Electrical Engineering and Computer Science

National Chiao Tung University

in partial Fulfillment of the Requirements

for the Degree of

Master

in

Communication Engineering

June 2007

Hsinchu, Taiwan, Republic of China

中華民國 96 年 6 月

# 在信號源不足環境下手機的定位和軌跡追蹤演算法

研究生：林育群

指導教授：方凱田

國立交通大學電信工程學系

電信研究所碩士班

## 摘要

手機的定位和軌跡追蹤在近年來受到相當高的注意。手機和基地台之間傳送的無線電訊號，在一般的網路定位估測機制下被廣泛地使用。此外，定位估測器加上卡曼爾濾波(Kalman filtering)的技術，可同時獲得位置的估測並且追蹤手機的軌跡。然而，這些已經存在的估測機制，在信號源不足(基地台數目小於三)的情況下，會變得無法計算並預測手機的位置跟軌跡。在此篇論文中，有兩種可預測的定位和軌跡追蹤演算法被提出來解決這個問題。預測定位追蹤機制(Predictive Location Tracking (PLT) scheme) 利用從卡曼爾濾波器(Kalman Filter)的預測訊息，提供給定位估測器當作是額外的訊號輸入，彌補訊號源不足而無法計算的問題。更進一步，地理輔助的預測定位追蹤機制(Geometric-assisted Predictive Location Tracking (GPLT) scheme)更加入了幾何精度稀釋(Geometric Dilution of Precision (GDOP))的資訊到演算法裡。採用所提出的地理輔助的預測定位追蹤(GPLT)機制在手機的定位追蹤上都可獲得更好的正確率，特別是當訊號源不足的時候。在此篇論文中有許多模擬的結果來證明地理輔助的預測定位追蹤(GPLT)機制跟其他兩種網路定位追蹤機制比較，可以獲得較高的正確率和穩定性。

# Wireless Location Tracking Algorithms for Environments with Insufficient Signal Sources

Student: Yu-Chun Lin

Advisor: Kai-Ten Feng

Department of Communication Engineering  
National Chiao Tung University

## Abstract

Location estimation and tracking for the mobile devices have attracted a significant amount of attention in recent years. The network-based location estimation schemes have been widely adopted based on the radio signals between the mobile device and the base stations. The location estimators associated with the Kalman filtering techniques are exploited to both acquire location estimation and trajectory tracking for the mobile devices. However, most of the existing schemes become unapplicable for location tracking due to the deficiency of signal sources. In this thesis, two predictive location tracking algorithms are proposed to alleviate this problem. The Predictive Location Tracking (PLT) scheme utilizes the predictive information obtained from the Kalman filter in order to provide the additional signal inputs for the location estimator. Furthermore, the Geometric-assisted Predictive Location Tracking (GPLT) scheme incorporates the Geometric Dilution of Precision (GDOP) information into the algorithm design. Persistent accuracy for location tracking can be achieved by adopting the proposed GPLT scheme, especially with inadequate signal sources. Numerical results demonstrate that the GPLT algorithm can achieve better precision in comparison with other network-based location tracking schemes.

## 誌謝

本篇論文的完成，誠摯地感謝我的指導老師 方凱田 博士，從踏入交通大學電信所開始，多虧老師的循循善誘，不但給予我在課業、研究上的幫助，使我學到了分析問題及解決問題的能力。在此，僅向老師及老師的家人致上最高的感謝之意。

感謝在電信研究所的日子裡，實驗室所提供完善的研究資源。承蒙仲賢和建華學長的提攜與照顧。而實驗室的同伴，文俊、柏軒跟裕彬，還有學弟們林志、伯泰、信龍跟瑜智，在課業上的砥礪與生活上的幫助也讓我在忙碌的研究所生涯中仍舊擁有快樂的心情。大學朋友和我的室友，志剛、柏昇、介遠、耀鈞和政達等，平日陪我打球運動，有空的時候出去玩樂，使得研究生生活不只是只有苦悶，也多了許多的回憶。

最後，感謝我的家人和我的女朋友仁雅，溫暖的家一直是我求學生涯中最強而有力的後盾，感謝你們的努力讓我能夠無後顧之憂地汲取知識，繼續升學。僅將本論文獻給我敬愛的父母，林連進先生、莊豔芬女士。

林育群

民國九十六年六月於新竹

# Contents

<b>1</b>	<b>Introduction</b>	<b>3</b>
<b>2</b>	<b>Preliminary studies and Related Work</b>	<b>8</b>
2.1	Mathematical Modeling . . . . .	8
2.2	Sources of Ranging Errors . . . . .	9
2.3	Studies on Existing Location Estimation Algorithms . . . . .	10
2.3.1	Two-Step Least Square . . . . .	13
2.4	Studies on Existing Location Tracking Algorithms . . . . .	17
2.4.1	Kalman Filtering . . . . .	17
2.4.2	Kalman Tracking (KT) Algorithm . . . . .	18
2.4.3	Cascade Location Tracking (CLT) Algorithm . . . . .	21
<b>3</b>	<b>Architectural Overview of the Proposed PLT and GPLT Algorithms</b>	<b>22</b>
<b>4</b>	<b>Formulation of the PLT Algorithm</b>	<b>27</b>
4.1	The Two-BSs Case . . . . .	29
4.2	The Single-BS Case . . . . .	30
<b>5</b>	<b>Formulation of the GPLT Algorithm</b>	<b>33</b>
5.1	The Geometric Dilution of Precision (GDOP) . . . . .	33
5.2	The Two-BSs Case . . . . .	34
5.2.1	The Computation of the Angle $\theta_k$ . . . . .	35
5.2.2	The Selection of the Distance $r_{v_1,k}^{GPLT}$ . . . . .	36

5.3	The Single-BS Case . . . . .	40
<b>6</b>	<b>Performance Evaluation</b>	<b>42</b>
6.1	The Noise Models and the Simulation Parameters . . . . .	42
6.2	Validation of the GPLT Scheme . . . . .	43
6.2.1	Validation with Angle Effect . . . . .	43
6.2.2	Validation with Distance Effect . . . . .	47
6.3	Simulation Results . . . . .	48
<b>7</b>	<b>Conclusion</b>	<b>55</b>



# Chapter 1

## Introduction

Wireless location technologies, which are designated to estimate the position of a Mobile Station (MS), have drawn a lot of attention over the past few decades. The Quality-of-Service (QoS) of the positioning accuracy has been announced after the issue of the emergency 911 (E-911) subscriber safety service [1]. With the assistance of the information derived from the positioning system, the required performance and objectives for the targeting Mobile Station (MS) can be achieved with augmented robustness. In recent years, there are increasing demands for commercial applications to adopt the location information within their system design, such as the navigation systems, the location-based billing, the health care systems, the Wireless Sensor Networks (WSNs) [2]- [4], and the Intelligent Transportation Systems (ITS) [5] [6]. With the emergent interests in the Location-Based Services (LBSs), the location estimation algorithms with enhanced precision become necessitate for the applications under different circumstances.

A variety of wireless location techniques have been investigated [7]- [10]. To simplify the introduction of these techniques, in the following we use two-dimensional (2D) cases as application examples. The network-based location estimation schemes have been widely proposed and employed in the wireless communication system. These schemes locate the position of a MS based on the measured radio signals from its neighborhood Base Stations (BSs). The representative algorithms for the network-based location estimation techniques



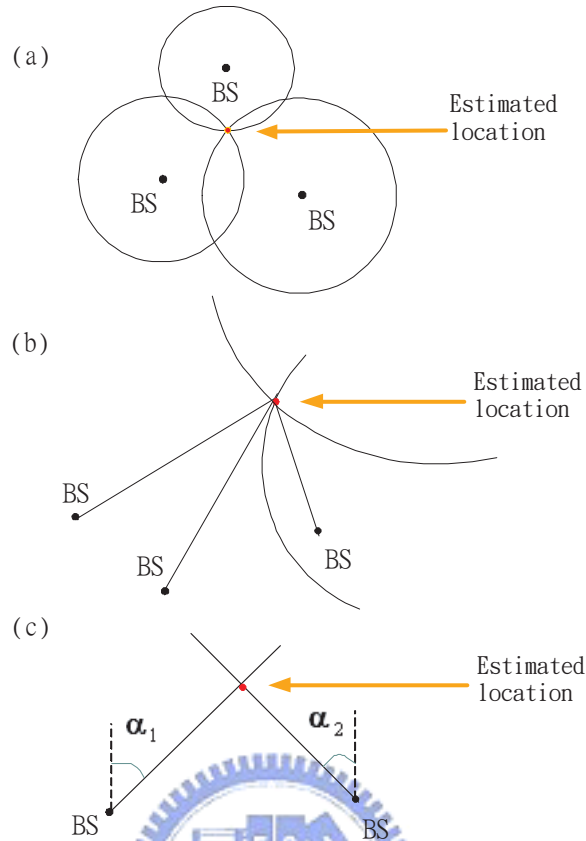


Figure 1.1: Position Determination Methods: (a) Time of Arrival (b)Time Difference of Arrival (c) Angel of Arrival

are the Time-Of-Arrival (TOA), the Time Difference-Of-Arrival (TDOA), and the Angle-Of-Arrival (AOA). The TOA scheme measures the arrival time of the radio signals coming from different wireless BSs, as shown in Fig. 1.1a; while the TDOA scheme measures the time difference between the radio signals, as shown in Fig. 1.1b. The AOA technique is conducted within the BS by observing the arriving angle of the signals coming from the MS, as shown in Fig. 1.1c.

It is recognized that the equations associated with the network-based location estimation schemes are inherently nonlinear. The uncertainties induced by the measurement noises make it more difficult to acquire the estimated MS position with tolerable precision. The Taylor Series Expansion (TSE) method was utilized in [11] to acquire the location estimation of the MS from the TOA measurements. The method requires iterative processes to obtain the

location estimate from a linearized system. The major drawback of the TSE scheme is that it may suffer from the convergence problem due to an incorrect initial guess of the MS's position. The two-step LS method was adopted to solve the location estimation problem from the TOA [12], the TDOA [13], and the TDOA/AOA measurements [14]. It is an approximate realization of the Maximum Likelihood (ML) estimator and does not require iterative processes. The two-step Least Square (LS) scheme is advantageous in its computational efficiency with adequate accuracy for location estimation. Instead of utilizing the Circular Line of Position (CLOP) methods (e.g. the TSE and the two-step LS schemes), the Linear Line of Position (LLOP) approach is presented as a new interpretation for the cell geometry from the TOA measurements. Since the pairwise intersections of  $N$  TOA measurements will establish  $(N - 1)$  independent linear lines, the LS method can therefore be applied to estimate the position of the MS. The detail algorithm of the LLOP approach can be obtained by using the TOA measurements as in [15], and the hybrid TOA/AOA measurements in [16].

In addition to the estimation of a MS's position, trajectory tracking of a moving MS has been studied [17] - [21]. The technique by combining the Kalman filter with the Weighted Least Square (WLS) method is exploited in [17]. The Kalman Tracking (KT) scheme [18] [19] distinguishes the linear part from the originally nonlinear equations for location estimation. The linear aspect is exploited within the Kalman filtering formulation; while the nonlinear term is served as an external measurement input to the Kalman filter. The technique utilized in [20] adopted the Kalman filters for both pre-processing and post-processing in order to both mitigate the Non-Line-of-Sight (NLOS) noises and track the MS's trajectory. The Cascade Location Tracking (CLT) scheme as proposed in [21] utilizes the two-step LS method for initial location estimation of the MS. The Kalman filtering technique is employed to smooth out and to trace the position of the MS based on its previously estimated data.

The Geometric Dilution of Precision (GDOP) [22] [23] and the Cramér-Rao Lower Bound (CRLB) [24] are the well-adopted metrics for justifying the accuracy of location estimation based on the geometric layouts between the MS and its associated BSs. It has been indicated in [25] that the environments with ill-conditioned layouts will result in relatively larger

GDOP and CRLB values. In general, the ill-conditioned situations can be classified into two categories: (i) insufficient number of available neighborhood BSs around the MS; and (ii) the occurrence of collinearity or coplanarity between the BSs and the MS. It is noticed that the problem caused by case (ii) can be resolved with well-planned locations of the BSs. Nevertheless, the scenarios with insufficient signal sources (i.e. case (i)) can happen in real circumstances, e.g. under rural environments or city valley with blocking buildings. It will be beneficial to provide consistent accuracy for location tracking under various environments. However, the wireless location tracking problem with deficient signal sources has not been extensively addressed in previous studies. In the cellular-based networks, three BSs are required in order to provide three signal sources for the TOA-based location estimation. The scheme as proposed in [26] considers the location tracking problem under the circumstances with short periods of signal deficiency, i.e. occasionally with only two signal sources available. The linear predictive information obtained from the Kalman filter is injected into its original LS scheme while one of the BSs is not observable. However, this algorithm is regarded as a preliminary design for signal deficient scenarios, which does not consider the cases while only one BS is available for location estimation. Insufficient accuracy for location estimation and tracking of the MS is therefore perceived.

In this thesis, a Predictive Location Tracking (PLT) algorithm is proposed to improve the problem with insufficient measurement inputs, i.e. with only two BSs or a single BS available to be exploited. The predictive information obtained from the Kalman filter is adopted as the virtual signal sources, which are incorporated into the two-step LS method for location estimation and tracking. Moreover, a Geometric-assisted Predictive Location Tracking (GPLT) scheme is proposed by adopting the Geometric Dilution of Precision (GDOP) [22] concept into its formulation in order to further enhance the performance of the original PLT algorithm. The position of the virtual signal sources are relocated for the purpose of achieving the minimum GDOP value associated with the MS's position. Along with the acquisition of the optimal location for the virtual signal source, the corresponding estimation and tracking errors acquired by using the proposed GPLT scheme can therefore be reduced. Moreover,

consistent precision for location tracking of a MS is also observed by exploiting the GPLT algorithm. Comparing with the existing techniques, the simulation results show that the proposed GPLT scheme can acquire higher accuracy for location estimation and tracking even under the situations with inadequate signal sources.

The remainder of this thesis is organized as follows. The related work, including the mathematic modeling, the sources of ranging errors, and other existing location estimation algorithms, is briefly described in chapter 2. The overview and motivations of the proposed Predictive Location Tracking (PLT) and Geometric-assisted Predictive Location Tracking (GPLT) schemes are explained in chapter 3. Chapter 4 presents the PLT algorithm with two different scenarios; while the formulation of the GPLT scheme is exploited in chapter 5. Chapter 6 illustrates the performance evaluation of the proposed GPLT and the PLT schemes in comparison with the existing location tracking techniques. Chapter 7 draws the conclusions.



## Chapter 2

# Preliminary studies and Related Work

### 2.1 Mathematical Modeling

In order to facilitate the design of the proposed PLT and the GPLT algorithms, the signal model for the TOA measurements is utilized. The set  $\mathbf{r}_k$  contains all the available measured relative distance at the  $k^{th}$  time step, i.e.  $\mathbf{r}_k = \{r_{1,k}, \dots, r_{i,k}, \dots, r_{N_k,k}\}$ , where  $N_k$  denotes the number of available BSs at the time step  $k$ . The measured relative distance ( $r_{i,k}$ ) between the MS and the  $i^{th}$  BS (obtained at the  $k^{th}$  time step) can be represented as

$$r_{i,k} = c \cdot t_{i,k} = \zeta_{i,k} + n_{i,k} + e_{i,k} \quad i = 1, 2, \dots, N_k \quad (2.1)$$

where  $t_{i,k}$  denotes the TOA measurement obtained from the  $i^{th}$  BS at the  $k^{th}$  time step, and  $c$  is the speed of light.  $r_{i,k}$  is contaminated with the TOA measurement noise  $n_{i,k}$  and the Non-line-of-sight (NLOS) error  $e_{i,k}$ . It is noted that the measurement noise  $n_{i,k}$  is in general considered as zero mean with Gaussian distribution. On the other hand, the NLOS error  $e_{i,k}$  is modeled as exponentially-distributed for representing the positive bias due to the non-line-of-sight effect [27] [28]. The noiseless relative distance  $\zeta_{i,k}$  (in (2.1)) between the MS's true

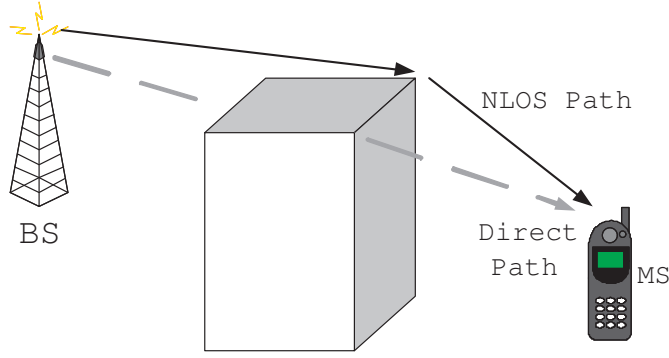


Figure 2.1: Geometry of the NLOS Error

position and the  $i^{th}$  BS can be obtained as

$$\zeta_{i,k} = [(x_k - x_{i,k})^2 + (y_k - y_{i,k})^2]^{\frac{1}{2}} \quad (2.2)$$

where  $\mathbf{x}_k = [x_k \ y_k]$  represents the MS's true position and  $\mathbf{x}_{i,k} = [x_{i,k} \ y_{i,k}]$  is the location of the  $i^{th}$  BS for  $i = 1$  to  $N_k$ . Therefore, the set of all the available BSs at the  $k^{th}$  time step can be obtained as  $\mathbf{P}_{BS,k} = \{\mathbf{x}_{1,k}, \dots, \mathbf{x}_{i,k}, \dots, \mathbf{x}_{N_k,k}\}$ .

## 2.2 Sources of Ranging Errors

The location accuracy can be reduced due to the influence of the measurement noises. Several main sources of ranging errors are described in this section, which are referred to [29].

### Non-Line-of-Sight Errors

In dense urban environment, there may be no direct path from the MS to the BS as shown in Fig. 2.1. Due to reflection and diffraction, the propagating wave may actually travel excess path lengths on the order of hundreds of meters and the direct path is blocked. This phenomenon, which we refer to as the NLOS error, ultimately translates into a biased estimate of the mobile's location. This problem has been recognized as a killer issue for mobile location. In order to mitigate the effect of the measurement bias, it is necessary to develop location algorithms that are robust to the NLOS error.

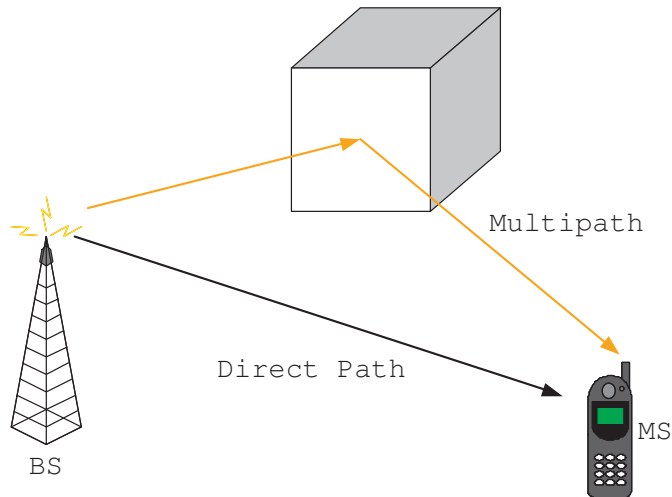


Figure 2.2: Multiple Reflections Arrive at the MS with Different Time Delays

### Multipath Errors

Multipath effects are caused by reflected signals entering the receiver antenna along with direct path signal, as shown in Fig. 2.2. Since the reflected path is longer than the direct path, the multipath signal blurs the peak of the direct signal at the output of the receiver correlation channel and distorts the pseudorange measurement.

### Receiver Measurement Processing

Advances in digital processing technology have enabled the implementation of small, affordable multiple channel receivers for parallel tracking of more than the minimum reference points for navigation solutions. This technology, in conjunction with advances in the speed and precision of microprocessor computations, has resulted in great reductions in receiver range measurement processing errors.

## 2.3 Studies on Existing Location Estimation Algorithms

Different location estimation schemes have been proposed to acquire the MS's position. Various types of information (e.g. the signal traveling distance, the received angle of the signal, or the Receiving Signal Strength (RSS)) are involved to facilitated the algorithm design for

location estimation. The primary objectives in most of the location estimation algorithms are to obtain higher estimation accuracy with promoted computational efficiency. The super-resolution (or high-resolution) schemes are proposed as in [30] - [33]. The scheme studied in [30] considers arbitrary-located antennas and a particular covariance matrix within a noisy environment. The covariance matrix is composed of various types of properties, including gain, phase, frequency, polarization, and AOA information. The subspace method is proposed in the scheme generates these component estimates of the covariance matrix based on an eigen-analysis or eigen-composition. The most well-known super-resolution algorithm is the Multiple Signal Classification (MUSIC) [31], It is experimentally illustrated to be a robust solution for location estimation, especially for a near-far environment. However, it has also been shown in [32] and [33] that the drawbacks of the MUSIC approach include (i) comparably high sensitivity to large noise and (ii) its complexity in computation.

The beamforming system is a space-time processor that operates on the output of a sensor array. It provides spatial filtering capability by enhancing the amplitude of a coherent signal associated with surrounding noises. Since the conventional beamforming technique is sensitive to the estimation error for the MS's position, a combination of localization and beamforming is proposed as in [34]. It increases the robustness to location errors without sacrificing the computation efficiency. An enhanced algorithm for simultaneous multi-source beamforming and adaptive multi-target tracking is studied in [35]. The correlation between the adaptive minimum variance beamforming and the optimal source localization is also investigated and developed as in [36].

Instead of exploiting the spatial and temporal information of the signal, the location fingerprinting technique locates the MS based on the the RSS [37] [38]. The technique involves both the off-line and the on-line phases. A location grid that is related to a signal signature database for a specific service area is developed in the off-line phase; while a measured RSS vector at the MS is delivered to the central server to compare with the location grid in the on-line phase. In addition, a hybrid algorithm which combines the RF propagation loss model is proposed to both mitigate the requirement of the training data and to adjust the configuration



changes [39]. On the other hand, the ray-tracing and ray-launching techniques are the two ray optical approaches for location estimation. The radio signals that are launched from a transmitter and reflected or diffracted by various objects are aggregated in a receiver. The field strength and the signal propagation can therefore be predicted [40]; while [41] proposed an efficient algorithm for prediction. The three dimensional indoor radio propagation models are developed in [42] and [43]. Experimental formulas from extensive measurements of urban and suburban propagation losses are studied as in [44] [45].

There are also different approaches adopting linearized methods to acquire the computing efficiency while obtaining an approximate estimation of the MS's position. The Taylor Series Expansion (TSE) method was utilized in [46] to acquire the location estimation from the TDOA measurements. The method requires iterative processes to obtain the location estimate from a linearized system. The major drawback of this method is that it may suffer from the convergence problem due to an incorrect initial guess of the MS's position. The two-step LS method was adopted to solve the location estimation problem from the TOA [12], the TDOA [13], and the TDOA/AOA measurements [14]. It is an approximate realization of the Maximum Likelihood (ML) estimator and does not require iterative processes. The two-step LS scheme is advantageous in its computational efficiency with adequate accuracy for location estimation. However, the scheme is demonstrated to be feasible for acquiring the MS's position under the LOS situations.

Instead utilizing the Circular Line Of Position (CLOP) methods (e.g. the TSE and two-step LS schemes), the Linear Line Of Position (LLOP) approach is presented as a new interpretation for the cell geometry from the TOA measurements. Since two TOA measurements that intersect at two points will generate a connecting line, two independent lines will be created by using three BSs in the scenario of two-dimensional location estimation. Therefore, the LS method can be adopted to estimate the location of the MS. The detail algorithm of the LLOP approach can be obtained by using the TOA measurements as in [15], and the hybrid TOA/AOA measurements in [16].

Some well-known schemes are improved continuously in order to achieve higher accu-

racy or promote the computational efficiency. The famous linear time-based algorithms, the Taylor-Series Estimation (TSE) [46], the two-step LS method, and the Linear Line-of-Position (LLOP) [15], are briefly described in the following subsection. For simplification, the thesis only described the two-step LS method in two-dimensional plane.

### 2.3.1 Two-Step Least Square

The content of this section will show the Two-step Least Square (two-step LS) location algorithm for TOA measurements and it can be obtained in [12]. For simplification, the two-step LS method will be described for TOA measurements in a two-dimensional (2-D) plane. The two-step LS method for TDOA measurements can be derived from the similar concept.

Assuming that  $(x_k, y_k)$  is the position of the mobile device,  $(x_{i,k}, y_{i,k})$  is the position of the  $i^{th}$  BS and  $r_{i,k}$  is the TOA measurement from the  $BS_i$ . Since in practice, especially in urban or in mountainous areas, the signals from the mobile device are usually unable to arrive at the base stations directly (or in the opposite direction), they always take a longer path than the direct one. So by incorporating the influences of NLOS propagation, killer issue for location estimation, on the location estimation, there exists

$$r_{i,k}^2 \geq (x_{i,k} - x_k)^2 + (y_{i,k} - y_k)^2 = \kappa_{i,k} - 2x_{i,k}x_k - 2y_{i,k}y_k + x_{i,k}^2 + y_{i,k}^2 \quad i = 1, 2, \dots, N \quad (2.3)$$

where  $\kappa_{i,k} = x_{i,k}^2 + y_{i,k}^2$ .  $r_{i,k} = ct_{i,k}$  is the measured distance between the MS and the  $i$ th BS, and  $c$  is the speed of light. By defining a new variable  $\beta_k^{(1)} = x_k^{(1)2} + y_k^{(1)2}$ , we rewrite (2.3) through a set of linear expressions

$$-2x_{i,k}x_k - 2y_{i,k}y_k + \beta_k \leq r_{i,k}^2 - \kappa_{i,k} \quad i = 1, 2, \dots, N \quad (2.4)$$

Let  $\mathbf{z}_k^{(1)} = [\hat{x}_k^{(1)} \quad \hat{y}_k^{(1)} \quad \hat{\beta}_k^{(1)}]^T$  and express (2.4) in matrix form

$$\mathbf{H}_k \mathbf{z}_k^{(1)} \leq \mathbf{J}_k \quad (2.5)$$

where

$$\mathbf{H}_k = \begin{bmatrix} -2x_{1,k} & -2y_{1,k} & 1 \\ -2x_{2,k} & -2y_{2,k} & 1 \\ \cdot & \cdot & \cdot \\ -2x_{N,k} & -2y_{N,k} & 1 \end{bmatrix} \quad \mathbf{J}_k = \begin{bmatrix} r_{1,k}^2 - \kappa_{1,k} \\ r_{2,k}^2 - \kappa_{2,k} \\ \cdot \\ r_{N,k}^2 - \kappa_{N,k} \end{bmatrix}$$

With measurement noise, the error vector is

$$\psi_k = \mathbf{J}_k - \mathbf{H}_k \mathbf{z}_k^{(1)} \quad (2.6)$$

When  $r_{i,k}$  can be expressed as  $\xi_{i,k} + cn_{i,k}$ , the error vector  $\psi_k$  is found to be

$$\begin{aligned} \psi_k &= 2c\mathbf{B}_k \mathbf{n}_k + c^2 \mathbf{n}_k \odot \mathbf{n}_k \\ \mathbf{B}_k &= \text{diag}\{\xi_{1,k}, \xi_{2,k}, \dots, \xi_{N,k}\} \end{aligned} \quad (2.7)$$

The symbol  $\odot$  represents the Schur product (element-by-element product). In addition, the second term on the right of (2.7) can be ignored since the condition  $cn_{i,k} \leq \xi_{i,k}$  is usually satisfied. As a result,  $\psi_k$  becomes a Gaussian random vector with covariance matrix given by

$$\Psi_k = E[\psi_k \psi_k^T] = 4c^2 \mathbf{B}_k \mathbf{Q}_k \mathbf{B}_k \quad (2.8)$$

$\mathbf{Q}_k$  is the covariance matrix of measured noise, and  $\xi_{1,k}, \dots, \xi_{N,k}$  are denoted as the true values of distances between the sources and the receiver. The element  $\mathbf{x}_k^{(1)}$  are related by the equation,  $\beta_k^{(1)} = x_k^{(1)2} + y_k^{(1)2}$ , which means that (2.5) is still a set of nonlinear equations in two variables  $x_k$  and  $y_k$ . The approach to solve the nonlinear problem is to first assume that there is no relationship among  $x_k^{(1)}$ ,  $y_k^{(1)}$  and  $\beta_k^{(1)}$ . That can then be solved by Least Square (LS). The final solution is obtained by imposing the known relationship to the computed result via another LS computation. This two step procedure is an approximation of a true ML

estimator. By considering the elements of  $\mathbf{x}_k^{(1)}$  independent, the ML estimator of  $\mathbf{x}_k^{(1)}$  is

$$\begin{aligned}\mathbf{x}_k^{(1)} &= \arg \min\{(\mathbf{J}_k - \mathbf{H}_k \mathbf{x}_k)^T \Psi_k^{-1} (\mathbf{J}_k - \mathbf{H}_k \mathbf{x}_k)\} \\ &= (\mathbf{H}_k^T \Psi_k^{-1} \mathbf{H}_k)^{-1} \mathbf{H}_k^T \Psi_k^{-1} \mathbf{J}_k\end{aligned}\quad (2.9)$$

The covariance matrix of  $\mathbf{x}_k^{(1)}$  is obtained by evaluating the expectations of  $\mathbf{x}_k^{(1)}$  and  $(\mathbf{x}_k^{(1)})(\mathbf{x}_k^{(1)})^T$  from (2.9). The covariance matrix of  $\mathbf{x}_k^{(1)}$  can be calculated as [13]

$$\text{cov}(\mathbf{x}_k^{(1)}) = (\mathbf{H}_k^T \Psi_k^{-1} \mathbf{H}_k)^{-1} \quad (2.10)$$

Since we have used the independent supposition of variables  $\hat{x}_k^{(1)}$ ,  $\hat{y}_k^{(1)}$ , and  $\hat{\beta}_k^{(1)}$  in the estimation of  $\mathbf{x}_k^{(1)}$  though the variable  $\hat{\beta}_k^{(1)}$  is dependent on the variable  $\hat{x}_k^{(1)}$  and  $\hat{y}_k^{(1)}$ , we should revise the results as follows. Let the estimation errors of  $\hat{x}_k^{(1)}$ ,  $\hat{y}_k^{(1)}$ , and  $\hat{\beta}_k^{(1)}$  be  $e_{1,k}$ ,  $e_{2,k}$ , and  $e_{3,k}$ . Here and below, denote the  $\ell^{\text{th}}$  entry of a matrix M as  $[M]_\ell$ ; then the entries in vector  $\mathbf{x}_k^{(1)}$  become

$$[\mathbf{x}_k^{(1)}]_1 = x_o + e_{1,k} \quad (2.11a)$$

$$[\mathbf{x}_k^{(1)}]_2 = y_o + e_{2,k} \quad (2.11b)$$

$$[\mathbf{x}_k^{(1)}]_3 = \beta_o + e_{3,k} \quad (2.11c)$$

where  $x_o$ ,  $y_o$ , and  $\beta_o$  are denoted as the true values of  $\hat{x}_k^{(1)}$ ,  $\hat{y}_k^{(1)}$ , and  $\hat{\beta}_k^{(1)}$ . Let another error vector

$$\psi'_k = \mathbf{J}'_k - \mathbf{H}'_k \mathbf{x}_k^{(2)} \quad (2.12)$$

where

$$\mathbf{H}'_k = \begin{bmatrix} 1 & 0 \\ 0 & 1 \\ 1 & 1 \end{bmatrix} \quad \mathbf{J}'_k = \begin{bmatrix} [\mathbf{x}_k^{(1)}]_1^2 \\ [\mathbf{x}_k^{(1)}]_2^2 \\ [\mathbf{x}_k^{(1)}]_3 \end{bmatrix}$$

and  $\mathbf{x}_k^{(2)} = \begin{bmatrix} \hat{x}_k^{(2)^2} \\ \hat{y}_k^{(2)^2} \end{bmatrix}$ . Substituting 2.11a- 2.11c into 2.12, we have

$$[\psi_k]_1 = 2x_o e_{1,k} + e_{1,k}^2 \approx 2x_o e_{1,k}$$

$$[\psi_k]_2 = 2y_o e_{2,k} + e_{2,k}^2 \approx 2y_o e_{2,k}$$

$$[\psi_k]_3 = e_{3,k}$$

Obviously, the above approximations are valid only when the errors  $e_{1,k}$ ,  $e_{2,k}$ , and  $e_{3,k}$  are fairly small. Subsequently, the covariance matrix of  $\psi'$  is

$$\begin{aligned} \Psi'_k &= E[\psi'_k \psi_k'^T] = 4\mathbf{B}'_k \text{cov}(\mathbf{x}_k^{(1)}) \mathbf{B}'_k \\ \mathbf{B}'_k &= \text{diag}\{x_o, y_o, 0.5\} \end{aligned} \quad (2.14)$$

As an approximation, elements  $x_o$  and  $y_o$  in matrix  $\mathbf{B}'_k$  can be replaced by the first two elements  $\hat{x}_k^{(1)}$  and  $\hat{y}_k^{(1)}$  in  $\mathbf{x}_k^{(1)}$ . Similarly, the ML estimate of  $\mathbf{x}_k^{(2)}$  is given by

$$\mathbf{x}_k^{(2)} = (\mathbf{H}'_k{}^T \Psi_k'^{-1} \mathbf{H}'_k{}^{-1}) \mathbf{H}'_k{}^T \Psi_k'^{-1} \mathbf{J}'_k \quad (2.15)$$

$$\approx (\mathbf{H}'_k{}^T \mathbf{B}'_k{}^{-1} (\text{cov}(\mathbf{x}_k^{(1)}))^{-1} \mathbf{B}'_k{}^{-1} \mathbf{H}'_k{}^{-1}) \quad (2.16)$$

$$\bullet (\mathbf{H}'_k{}^T \mathbf{B}'_k{}^{-1} (\text{cov}(\mathbf{x}_k^{(1)}))^{-1} \mathbf{B}'_k{}^{-1}) \mathbf{J}'_k \quad (2.17)$$

So the final position estimation  $\mathbf{z}_k = [\hat{x}_k \quad \hat{y}_k]^T$  is

$$\mathbf{z}_k = \sqrt{\mathbf{x}_k^{(2)}}, \quad \text{or} \quad \mathbf{z}_k = -\sqrt{\mathbf{x}_k^{(2)}} \quad (2.18)$$

Here the sign of  $\hat{x}_k$  should coincide with the sign of  $[\mathbf{x}_k^{(1)}]_1$  calculated by solving (2.9), and the sign of  $\hat{y}_k$  coincides with the sign of  $[\mathbf{x}_k^{(1)}]_2$ .

The complete derivation of the two-step LS for TOA measurements is shown above. In addition, the two-step LS method can be adopted to estimate MS location from the TDOA [13], and the TDOA/AOA measurements [14]. The following two subsections describe the 3-D

TOA location estimation for the satellite-based system, and the 3-D TDOA/AOA location estimation algorithm for the cellular network.

## 2.4 Studies on Existing Location Tracking Algorithms

### 2.4.1 Kalman Filtering

Kalman Filtering method is always utilized for location tracking because it utilizes the state vector with the position, the velocity, and the acceleration of the MS to record and predict the MS's trajectory. The measurement and state equations for the Kalman filter can be represented as

$$z_k = \mathbf{M}\hat{\mathbf{s}}_k + \mathbf{m}_k \quad (2.19)$$

$$\hat{\mathbf{s}}_k = \mathbf{F}\hat{\mathbf{s}}_{k-1} + \mathbf{p}_k \quad (2.20)$$

The matrix  $\mathbf{M}$  in the measurement equation (2.19) relates the state to the measurement  $z_k$ . The matrix  $\mathbf{F}$  in the equation (2.20) relates the state at the previous time step  $k-1$  to the state at the current step  $k$ . The variables  $\mathbf{m}_k$  and  $\mathbf{p}_k$  denote the measurement and the process noises associated with the covariance matrices  $\mathbf{R}$  and  $\mathbf{Q}$  within the Kalman filtering formulation.

The Kalman filter estimates a process by using a form of feedback control: the filter estimates the process state at some time and then obtains feedback in the form of (noisy) measurements. As such, the equations of the Kalman filter fall into two groups: *time update* equations and *measurement update* equations. The time update equations are as following

$$\hat{\mathbf{s}}_{k|k-1} = \mathbf{F}\hat{\mathbf{s}}_{k-1|k-1} \quad (2.21)$$

$$\mathbf{P}_{k|k-1} = \mathbf{F}\mathbf{P}_{k-1|k-1}\mathbf{F} + \mathbf{Q} \quad (2.22)$$

And the measurement update equations are shown

$$\mathbf{K}_k = \mathbf{P}_{k|k-1} \mathbf{M}^T (\mathbf{M} \mathbf{P}_{k|k-1} \mathbf{M}^T + \mathbf{R})^{-1} \quad (2.23)$$

$$\hat{\mathbf{s}}_{k|k} = \hat{\mathbf{s}}_{k|k-1} + \mathbf{K}_k (\mathbf{z}_k - \mathbf{M} \hat{\mathbf{s}}_{k|k-1}) \quad (2.24)$$

$$\mathbf{P}_{k|k} = (\mathbf{I} - \mathbf{K}_k \mathbf{M}) \mathbf{P}_{k|k-1} \quad (2.25)$$

The first task during the measurement update is to compute the Kalman gain,  $\mathbf{K}_k$ . The next step is to actually measure the process to obtain  $\mathbf{z}_k$ , and then to generate a *posteriori* state estimate by incorporating the measurement as in (2.24). The final step is to obtain a *posteriori* error covariance estimate via (2.25). The Kalman filter instead recursively conditions the current estimate on all of the past measurements.

#### 2.4.2 Kalman Tracking (KT) Algorithm

The Kalman Tracker [18], which is designed based on the TDOA measurements, considers the nonlinear term as an external measurement input to its Kalman filtering formulation. The Kalman Tracking method for TOA measurements can be derived from the similar concept. It distinguishes the linear part from the originally nonlinear equations for location estimation and tracking.

The difference between ranges of the  $i$ th BS and the reference BS can be defined as

$$r_{i,1,k} = r_{i,k} - r_{1,k} = c \cdot t_{i,1,k} \quad i = 2, \dots, N \quad (2.26)$$

where  $c$  is the propagation speed, and  $N$  is the number of active BSs.

The squared distance between the  $i$ th BS and the MS is equal to

$$r_{i,k}^2 = \|\mathbf{x}_{i,k} - \mathbf{x}_k\|^2 = \|\mathbf{x}_{i,k}\|^2 - 2\mathbf{x}_{i,k}^T \mathbf{x}_k + \|\mathbf{x}_k\|^2 \quad (2.27)$$

where  $\mathbf{x}_{i,k} = [\hat{x}_{i,k} \quad \hat{y}_{i,k}]^T$  and  $\mathbf{x}_k = [x_k \quad y_k]^T$  are the vectors which define the known position of the  $i$ th BS and unknown MS position.

These equations show a nonlinear relation between the TDOA measurements and the BS position. From (2.26), the squared distance between the  $i$ th BS and the MS can also be expressed as

$$r_{i,k}^2 = r_{i,1,k}^2 + 2r_{1,k}r_{i,1,k} + r_{1,k}^2 \quad (2.28)$$

Using equations (2.27) and (2.28), the linear system of equations is derived as

$$\mathbf{G}_k \mathbf{x}_k = \mathbf{u}_k - r_{1,k} \rho_k \quad (2.29)$$

where

$$\mathbf{G}_k = \begin{bmatrix} (x_{2,k} - x_{1,k}) & (y_{2,k} - y_{1,k}) \\ \dots & \dots \\ (x_{N,k} - x_{1,k}) & (y_{N,k} - y_{1,k}) \end{bmatrix}$$

$$\mathbf{u}_k = \frac{1}{2} \begin{bmatrix} \|\mathbf{x}_{2,k}\|^2 - \|\mathbf{x}_{1,k}\|^2 - r_{2,1,k}^2 \\ \dots \\ \|\mathbf{x}_{N,k}\|^2 - \|\mathbf{x}_{1,k}\|^2 - r_{N,1,k}^2 \end{bmatrix}$$

$$\rho_k = \begin{bmatrix} r_{2,1,k} \\ \dots \\ r_{N,1,k} \end{bmatrix}$$

The resulting linear equation also depends on a distance measurement  $r_{1,k}$ , proportional to the TOA between the reference BS and the MS, which has a nonlinear dependence on the BS co-ordinates.

In [18], a Kalman tracker based on TDOA measurements is derived from the linear equation (2.29). The use of the Kalman filter allows tracking the position and speed of the MS. The transition equation, defined for continuous movement, is linear

$$\hat{\mathbf{s}}_k = \mathbf{F} \hat{\mathbf{s}}_{k-1} + \mathbf{p}_k \quad (2.30)$$



where  $\hat{\mathbf{s}}_k = [\hat{x}_k \ \hat{y}_k \ \hat{v}_{x,k} \ \hat{v}_{y,k}]^T$  is the dynamic state vector, where its components represent the MS position and the speed in two-dimensional Cartesian co-ordinates at discrete time  $k$ . The matrix  $\mathbf{F}$  is the state matrix with  $\Delta$  equal to the time interval between samples

$$\mathbf{F} = \begin{bmatrix} 1 & 0 & \Delta & 0 \\ 0 & 1 & 0 & \Delta \\ 0 & 0 & 1 & 0 \\ 0 & 0 & 0 & 1 \end{bmatrix} \quad (2.31)$$

and  $\mathbf{p}(k) = [0 \ 0 \ p_{x,k} \ p_{y,k}]$  is the disturbance transition vector defined as a two-dimensional random speed vector with covariance matrix  $\mathbf{Q}$ .

From the linear equation (2.29), it can be defined the measurement equation that relates the state vector with the observation vector

$$\mathbf{z}_k = \mathbf{G}_k \hat{\mathbf{s}}_k + \mathbf{m}_k \quad (2.32)$$

where matrix  $\mathbf{G}_k$  is constant instead of the variable matrix derived for the Extended Kalman filter in [19] and the *update* equations are the same as that in the front subsection. The noise vector  $\mathbf{m}_k$  depends on the noise in the TDOA measurement

$$r_{i,1,k} = r_{i,1,k}^o + cn_{i,1,k} \quad i = 2, \dots, N \quad (2.33)$$

being  $r_{i,1,k}^o = ct_{i,1,k}^o$  obtained from the noise free value of the TDOA between the  $i$ th BS and the reference BS.

Substituting this expression in equation (2.29) and considering that in practice  $cn_{i,1,k} \ll r_{i,k}^o$  is usually satisfied, the measurement noise is found to be

$$\mathbf{m}_k = c\mathbf{B}_k \mathbf{n}_k \quad (2.34)$$

$$\mathbf{B}_k = \text{diag}\{r_{2,k}^o, r_{3,k}^o, \dots, r_{N,k}^o\} \quad (2.35)$$

with covariance matrix

$$\mathbf{C}_k = c^2 \mathbf{B}_k \mathbf{R}_k \mathbf{B}_k^T \quad (2.36)$$

$\mathbf{R}_k$  is the covariance matrix of the noise in the TDOA measurements defined from the variance of the noise in the time delay estimation from each BS

$$\mathbf{R}_k = \mathbf{H}_k \sigma_{TDOA}^2 \mathbf{H}_k^T \quad (2.37)$$

$\mathbf{H}_k$  is the  $(N-1) \times N$  matrix that defines the difference of times in the TDOA method

$$\mathbf{H}_k = \begin{bmatrix} -1 & 1 & 0 & \dots & 0 \\ -1 & 0 & 1 & \dots & 0 \\ \dots & \dots & \dots & \dots & \dots \\ -1 & 0 & 0 & \dots & 1 \end{bmatrix} \quad (2.38)$$

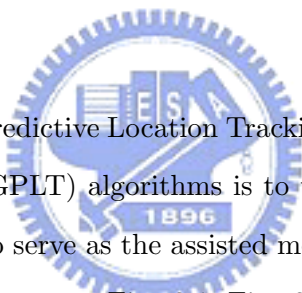
assuming that the measurements obtained are uncorrelated  $\sigma_{TDOA}^2$  is a diagonal matrix of dimension equal to the number of available measurements  $N$ .

### 2.4.3 Cascade Location Tracking (CLT) Algorithm

The Cascade Location Tracking (CLT) scheme as proposed in [21] utilizes the two-step Least Square (LS) method [12] [13] for initial location estimation of the MS. The two-step LS method computes the solution  $\mathbf{z}_k$  which is also the measurement input of Kalman filter. After the Kalman filter, we can get the final solution  $\hat{\mathbf{s}}_k$  of MS. The Kalman filtering technique is employed to smooth out and to trace the position of the MS based on its previously estimated data. The details of the two-step LS method and Kalman filter are illustrated in front sections.

## Chapter 3

# Architectural Overview of the Proposed PLT and GPLT Algorithms



The objective of the proposed Predictive Location Tracking (PLT) and the Geometric-assisted Predictive Location Tracking (GPLT) algorithms is to utilize the predictive information acquired from the Kalman filter to serve as the assisted measurement inputs while the environments are deficient with signal sources. Fig. 3.1, Fig. 3.2 and Fig. 3.3 illustrate the system architectures of the KT [18], the CLT [21] and the proposed PLT/GPLT schemes. The TOA signals ( $\mathbf{r}_k$  as in (2.1)) associated with the corresponding location set of the BSs ( $\mathbf{P}_{BS,k}$ ) are obtained as the signal inputs to each of the system, which result in the estimated state vector of the MS, i.e.  $\hat{\mathbf{s}}_k = [\hat{\mathbf{x}}_k \ \hat{\mathbf{v}}_k \ \hat{\mathbf{a}}_k]^T$  where  $\hat{\mathbf{x}}_k = [\hat{x}_k \ \hat{y}_k]$  represents the MS's estimated position,  $\hat{\mathbf{v}}_k = [\hat{v}_{x,k} \ \hat{v}_{y,k}]$  is the estimated velocity, and  $\hat{\mathbf{a}}_k = [\hat{a}_{x,k} \ \hat{a}_{y,k}]$  denotes the estimated acceleration.

Since the equations (i.e.(2.1) and (2.2)) associated with the network-based location estimation are intrinsically nonlinear, different mechanisms are considered within the existing algorithms for location tracking. The KT scheme [18] (as shown in Fig. 3.1) explores the linear aspect of location estimation within the Kalman filtering formulation; while the nonlinear term (i.e.  $\hat{\beta}_k = \hat{x}_k^2 + \hat{y}_k^2$ ) is treated as an additional measurement input to the Kalman

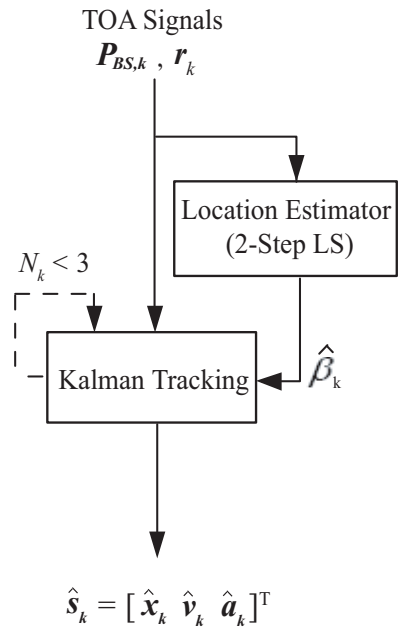


Figure 3.1: The Architecture Diagrams of the Kalman Tracking (KT) Scheme

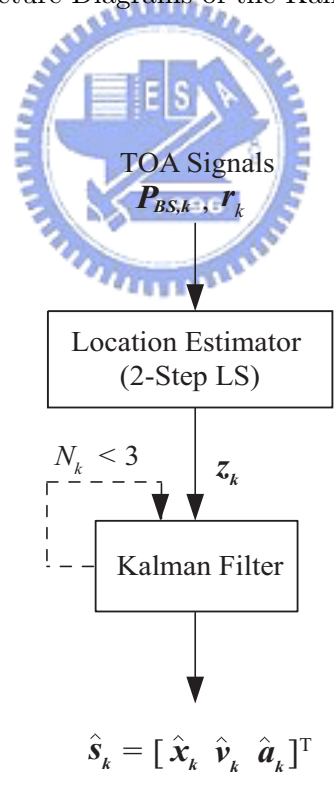


Figure 3.2: The Architecture Diagrams of the Cascade Location Tracking (CLT) Scheme

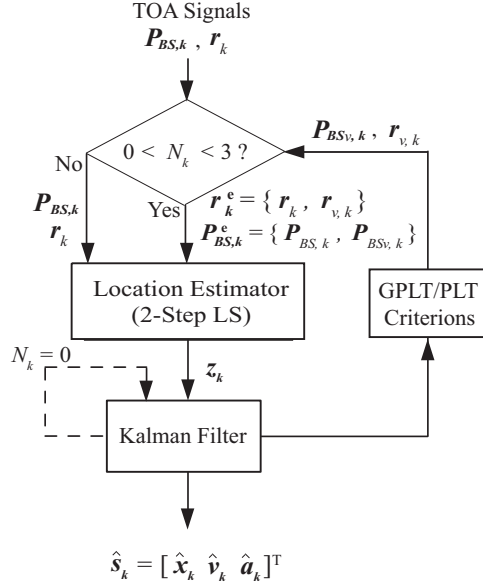


Figure 3.3: The Architecture Diagrams of the Proposed Predictive Location Tracking (PLT) and Geometric-assisted Predictive Location Tracking (GPLT) Scheme

filter. It is stated within the KT scheme that the value of the nonlinear term can be obtained from an external location estimator, e.g. via the two-step LS method. Consequently, the estimation accuracy of the KT algorithm greatly depends on the precision of the additional location estimator. On the other hand, the CLT scheme [21] (as illustrated in Fig. 3.2) adopts the two-step LS method to acquire the preliminary location estimate of the MS. The Kalman Filter is utilized to smooth out the estimation error by tracing the estimated state vector  $\hat{\mathbf{s}}_k$  of the MS.


The architecture of the proposed PLT and GPLT schemes is illustrated in Fig. 3.3. It is noticed that the GPLT algorithm involves additional transformation via the GDOP calculation comparing with the PLT scheme. It can be seen that the PLT/GPLT algorithms will be the same as the CLT scheme while  $N_k \geq 3$ , i.e. the number of available BSs is greater than or equal to three. On the other hand, the effectiveness of the PLT/GPLT schemes is revealed as  $1 \leq N_k < 3$ , i.e. with deficient measurement inputs. The predictive state information obtained from the Kalman filter is utilized for acquiring the assisted information, which will be fed back into the location estimator. The extended sets for the locations of the BSs (i.e.  $\mathbf{P}_{BS,k}^e = \{\mathbf{P}_{BS,k}, \mathbf{P}_{BSv,k}\}$ ) and the measured relative distances (i.e.  $\mathbf{r}_k^e = \{\mathbf{r}_k, \mathbf{r}_{v,k}\}$ ) will be

utilized as the inputs to the location estimator. The sets of the virtual BS's locations  $\mathbf{P}_{BS_v,k}$  and the virtual measurements  $\mathbf{r}_{v,k}$  are defined as follows.

**Definition 1 (Virtual Base Stations)** *Within the PLT/GPLT formulation, the virtual Base Stations are considered as the designed locations for assisting the location tracking of the MS under the environments with deficient signal sources. The set of virtual BSs  $\mathbf{P}_{BS_v,k}$  is defined under two different numbers of  $N_k$  as*

$$\mathbf{P}_{BS_v,k} = \begin{cases} \{\mathbf{x}_{v_1,k}\} & \text{for } N_k = 2 \\ \{\mathbf{x}_{v_1,k}, \mathbf{x}_{v_2,k}\} & \text{for } N_k = 1 \end{cases} \quad (3.1)$$

**Definition 2 (Virtual Measurements)** *Within the PLT/GPLT formulation, the virtual measurements are utilized to provide assisted measurement inputs while the signal sources are insufficient. Associating with the designed set of virtual BSs  $\mathbf{P}_{BS_v,k}$ , the corresponding set of virtual measurements  $\mathbf{r}_{v,k}$  is defined as*

$$\mathbf{r}_{v,k} = \begin{cases} \{r_{v_1,k}\} & \text{for } N_k = 2 \\ \{r_{v_1,k}, r_{v_2,k}\} & \text{for } N_k = 1 \end{cases} \quad (3.2)$$


It is noticed that the major tasks of both the PLT and GPLT schemes are to design and to acquire the values of  $\mathbf{P}_{BS_v,k}$  and  $\mathbf{r}_{v,k}$  for the two cases (i.e.  $N_k = 1$  and  $2$ ) with inadequate signal sources. In both the KT and the CLT schemes, the estimated state vector  $\hat{\mathbf{s}}_k$  can only be updated by the internal prediction mechanism of the Kalman filter while there are insufficient numbers of BSs (i.e.  $N_k < 3$  as shown in Fig. 3.1 and 3.2 with the dashed lines). The location estimator (i.e. the two-step LS method) is consequently disabled owing to the inadequate number of the signal sources. The tracking capabilities of both schemes significantly depend on the correctness of the Kalman filter's prediction mechanism. Therefore, the performance for location tracking can be severely degraded due to the changing behavior of the MS, i.e. with the variations from the MS's acceleration.

On the other hand, the proposed PLT/GPLT algorithms can still provide satisfactory tracking performance with deficient measurement inputs, i.e. with  $N_k = 1$  and  $2$ . Under

these circumstances, the location estimator is still effective with the additional virtual BSs  $\mathbf{P}_{BS_v,k}$  and the virtual measurements  $\mathbf{r}_{v,k}$ , which are imposed from the predictive output of the Kalman filter (as shown in Fig. 3.3). It is also noted that the PLT/GPLT schemes will perform the same as the CLT method under the case with no signal input, i.e. under  $N_k = 0$ . Furthermore, the GPLT algorithm enhances the precision and the robustness of the location estimation from the PLT scheme by considering the GDOP effect, i.e. the geographic relationship between the locations of the BSs and the MS. By adopting the GPLT scheme, the locations of the virtual BSs  $\mathbf{P}_{BS_v,k}^{PLT}$  obtained from the PLT method are adjusted into  $\mathbf{P}_{BS_v,k}^{GPLT}$  in order to make the predicted MS possess with a minimal GDOP value. Consequently, smaller estimation errors can be acquired by exploiting the GPLT algorithm comparing with the PLT scheme. The virtual BS's location set  $\mathbf{P}_{BS_v,k}^{PLT}$  and the virtual measurements  $\mathbf{r}_{v,k}^{PLT}$  by exploiting the PLT formulation is presented in the next section; while the adjusted location set of the virtual BSs  $\mathbf{P}_{BS_v,k}^{GPLT}$  adopting from the GPLT algorithm will be derived in chapter 5.



## Chapter 4

# Formulation of the PLT Algorithm

The proposed Predictive Location Tracking (PLT) scheme will be explained in this section. As shown in Fig. 3.3, the measurement and state equations for the Kalman filter can be represented as

$$\mathbf{z}_k = \mathbf{M}\hat{\mathbf{s}}_k + \mathbf{m}_k \quad (4.1)$$

$$\hat{\mathbf{s}}_k = \mathbf{F}\hat{\mathbf{s}}_{k-1} + \mathbf{p}_k \quad (4.2)$$

where  $\hat{\mathbf{s}}_k = [\hat{\mathbf{x}}_k \ \hat{\mathbf{v}}_k \ \hat{\mathbf{a}}_k]^T$ . The variables  $\mathbf{m}_k$  and  $\mathbf{p}_k$  denote the measurement and the process noises associated with the covariance matrices  $\mathbf{R}$  and  $\mathbf{Q}$  within the Kalman filtering formulation. The measurement vector  $\mathbf{z}_k = [\hat{x}_{ls,k} \ \hat{y}_{ls,k}]^T$  represents the measurement input which is obtained from the output of the two-step LS estimator at the  $k^{th}$  time step (as in Fig. ??.(c)).



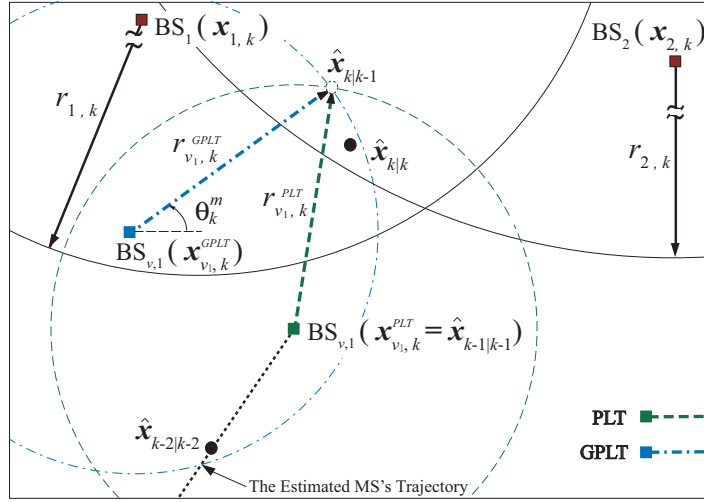


Figure 4.1: The Schematic Diagram of the Two-BSs Case for the proposed PLT and GPLT Schemes

The matrix  $\mathbf{M}$  and the state transition matrix  $\mathbf{F}$  can be obtained as

$$\mathbf{M} = \begin{bmatrix} 1 & 0 & 0 & 0 & 0 & 0 \\ 0 & 1 & 0 & 0 & 0 & 0 \end{bmatrix} \quad (4.3)$$

$$\mathbf{F} = \begin{bmatrix} 1 & 0 & \Delta t & 0 & \frac{1}{2}\Delta t^2 & 0 \\ 0 & 1 & 0 & \Delta t & 0 & \frac{1}{2}\Delta t^2 \\ 0 & 0 & 1 & 0 & \Delta t & 0 \\ 0 & 0 & 0 & 1 & 0 & \Delta t \\ 0 & 0 & 0 & 0 & 1 & 0 \\ 0 & 0 & 0 & 0 & 0 & 1 \end{bmatrix} \quad (4.4)$$

where  $\Delta t$  denotes the sample time interval. The main concept of the PLT scheme is to provide additional virtual measurements (i.e.  $\mathbf{r}_{v,k}$  as in (3.2)) to the two-step LS estimator while the signal sources are insufficient. Two cases (i.e. the two-BSs case and the single-BS case) are considered as follows:

## 4.1 The Two-BSs Case

As shown in Fig. 4.1, it is assumed that only two BSs (i.e. BS<sub>1</sub> and BS<sub>2</sub>) associated with two TOA measurements are available at the time step  $k$  in consideration. The main target is to introduce an additional virtual BS along with its virtual measurement (i.e.  $\mathbf{P}_{BS_v,k}^{PLT} = \{\mathbf{x}_{v_1,k}^{PLT}\}$  and  $\mathbf{r}_{v,k}^{PLT} = \{r_{v_1,k}^{PLT}\}$ ) by acquiring the predictive output information from the Kalman filter. Knowing that there are predicting and correcting phases within the Kalman filtering formulation, the predictive state can therefore be utilized to compute the supplementary virtual measurement  $r_{v_1,k}^{PLT}$  as

$$\begin{aligned} r_{v_1,k}^{PLT} &= \|\hat{\mathbf{x}}_{k|k-1} - \hat{\mathbf{x}}_{k-1|k-1}\| \\ &= \|\mathbf{M}\mathbf{F}\hat{\mathbf{s}}_{k-1|k-1} - \hat{\mathbf{x}}_{k-1|k-1}\| \end{aligned} \quad (4.5)$$

where  $\hat{\mathbf{x}}_{k|k-1}$  denotes the predicted MS's position at time step  $k$ ; while  $\hat{\mathbf{x}}_{k-1|k-1}$  is the corrected MS's position obtained at the  $(k-1)^{th}$  time step. It is noticed that both values are available at the  $(k-1)^{th}$  time step. The virtual measurement  $r_{v_1,k}^{PLT}$  is defined as the distance between the previous location estimate ( $\hat{\mathbf{x}}_{k-1|k-1}$ ) as the position of the virtual BS (i.e. BS<sub>v,1</sub>:  $\mathbf{x}_{v_1,k}^{PLT} \triangleq \hat{\mathbf{x}}_{k-1|k-1}$ ) and the predicted MS's position ( $\hat{\mathbf{x}}_{k|k-1}$ ) as the possible position of the MS (as shown in Fig. 4.1). It is also noted that the corrected state vector  $\hat{\mathbf{s}}_{k-1|k-1}$  is available at the current time step  $k$ ; while  $\hat{\mathbf{s}}_{k|k}$  is unobtainable at the  $k^{th}$  time step. By adopting  $r_{v_1,k}^{PLT}$  (in (4.5)) as the additional signal input, the measurement vector  $\mathbf{z}_k$  can be acquired after the three measurement inputs  $\mathbf{r}_k^e = \{r_{1,k}, r_{2,k}, r_{v_1,k}^{PLT}\}$  and the locations of the BSs  $\mathbf{P}_{BS,k}^e = \{\mathbf{x}_{1,k}, \mathbf{x}_{2,k}, \mathbf{x}_{v_1,k}^{PLT}\}$  have been imposed into the two-step LS estimator. Therefore, the state vector  $\hat{\mathbf{s}}_{k|k}$  can be obtained with the implementation of the correcting phase of the Kalman filter at the time step  $k$  as

$$\hat{\mathbf{s}}_{k|k} = \hat{\mathbf{s}}_{k|k-1} + \mathbf{P}_{k|k-1}\mathbf{M}^T[\mathbf{M}\mathbf{P}_{k|k-1}\mathbf{M}^T + \mathbf{R}]^{-1}(\mathbf{z}_k - \mathbf{M}\hat{\mathbf{s}}_{k|k-1}) \quad (4.6)$$

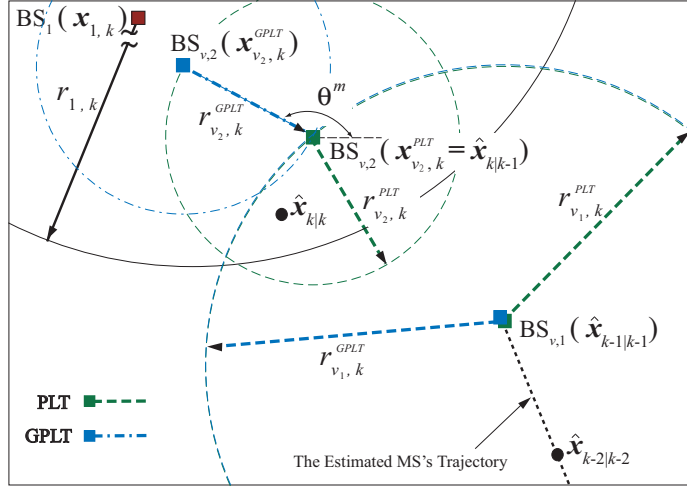


Figure 4.2: The Schematic Diagram of the Single-BS Case for the proposed PLT and GPLT Schemes

where

$$\mathbf{P}_{k|k-1} = \mathbf{F}\mathbf{P}_{k-1|k-1}\mathbf{F}^T + \mathbf{Q} \quad (4.7)$$

$$\mathbf{P}_{k-1|k-1} = [\mathbf{I} - \mathbf{P}_{k-1|k-2}\mathbf{M}^T(\mathbf{M}\mathbf{P}_{k-1|k-2}\mathbf{M}^T + \mathbf{R})^{-1}\mathbf{M}] \mathbf{P}_{k-1|k-2} \quad (4.8)$$

It is noted that  $\mathbf{P}_{k|k-1}$  and  $\mathbf{P}_{k-1|k-1}$  represent the predicted and the corrected estimation covariances within the Kalman filter.  $\mathbf{I}$  in (4.8) is denoted as an identity matrix. As can be observed from Fig. 4.1, the virtual measurement  $r_{v,1,k}^{PLT}$  associating with the other two existing measurements  $r_{1,k}$  and  $r_{2,k}$  provide a confined region for the estimation of the MS's location at the time step  $k$ , i.e.  $\hat{\mathbf{x}}_{k|k}$ .

## 4.2 The Single-BS Case

In this case, only one BS (i.e.  $BS_1$ ) with one TOA measurement input is available at the  $k^{th}$  time step (as shown in Fig.4.2). Two additional virtual BSs and measurements are required for the computation of the two-step LS estimator, i.e.  $\mathbf{P}_{BS_{v,k}}^{PLT} = \{\mathbf{x}_{v,1,k}^{PLT}, \mathbf{x}_{v,2,k}^{PLT}\}$  and  $\mathbf{r}_{v,k}^{PLT} =$

$\{r_{v_1,k}^{PLT}, r_{v_2,k}^{PLT}\}$ . Similar to the previous case, the first virtual measurement  $r_{v_1,k}^{PLT}$  is acquired as in (4.5) by considering  $\hat{\mathbf{x}}_{k-1|k-1}$  as the position of the first virtual BS (i.e.  $\mathbf{x}_{v_1,k}^{PLT} = \hat{\mathbf{x}}_{k-1|k-1}$ ) with the predicted MS's position (i.e.  $\hat{\mathbf{x}}_{k|k-1}$ ) as the possible position of the MS. On the other hand, the second virtual BS's position is assumed to locate at the predicted MS's position (i.e.  $\mathbf{x}_{v_2,k}^{PLT} \triangleq \hat{\mathbf{x}}_{k|k-1}$ ) as illustrated in Fig. 4.2. The corresponding second virtual measurement  $r_{v_2,k}^{PLT}$  is defined as the average prediction error obtained from the Kalman filtering formulation by accumulating the previous time steps as

$$r_{v_2,k}^{PLT} = \frac{1}{k-1} \sum_{i=1}^{k-1} \|\hat{\mathbf{x}}_{i|i} - \hat{\mathbf{x}}_{i|i-1}\| \quad (4.9)$$

It is noted that  $r_{v_2,k}^{PLT}$  is obtained as the mean prediction error until the  $(k-1)^{th}$  time step. In the case while the Kalman filter is capable of providing sufficient accuracy in its prediction phase, the virtual measurement  $r_{v_2,k}^{PLT}$  may approach zero value. Associating with the single measurement  $r_{1,k}$  from BS<sub>1</sub>, the two additional virtual measurements  $r_{v_1,k}^{PLT}$  (centered at  $\hat{\mathbf{x}}_{k-1|k-1}$ ) and  $r_{v_2,k}^{PLT}$  (centered at  $\hat{\mathbf{x}}_{k|k-1}$ ) result in a constrained region (as in Fig. 4.2) for location estimation of the MS under the environments with insufficient signal sources.

It is also noticed that the variations of the measurement inputs are the required information for adopting the two-step LS estimator. It utilizes the signal variation as an indicator to consider the weighting factor for a specific signal source, i.e. smaller weighting coefficient should be assigned to a measurement input if it encompasses comparably larger signal variations. The weighted least square algorithm can therefore be performed within the two-step LS estimator according to the designated weighting values associated with the signal sources. Similar concept can be exploited to assign the weighting coefficients for the virtual measurements. The virtual measurements can be represented as

$$r_{v_i,k} = \zeta_{v_i,k} + n_{v_i,k} \quad \text{for } i = 1, 2 \quad (4.10)$$

where  $\zeta_{v_i,k}$  is denoted as the deterministic noiseless virtual measurement; while  $n_{v_i,k}$  represents the *virtual noise* (i.e. the component with randomness) associated with the virtual

measurement  $r_{v_i,k}$ . Based on (4.5), the signal variation of  $r_{v_1,k}^{PLT}$  is considered as the variance of the predicted distance  $\|\hat{\mathbf{x}}_{k|k-1} - \hat{\mathbf{x}}_{k-1|k-1}\|$  between the previous  $(k-1)$  time steps. Therefore, the virtual noise can be regarded as zero mean with variance  $\sigma_{n_{v_1,k}}^2 = \text{Var}(r_{v_1,k}^{PLT}) = \text{Var}(\|\hat{\mathbf{x}}_{k|k-1} - \hat{\mathbf{x}}_{k-1|k-1}\|)$ . It is noted that the mean value of  $r_{v_i,k}^{PLT}$  is considered by the noiseless virtual measurement  $\zeta_{v_1,k}^{PLT}$ . Similarly, since the signal variation of the second virtual measurement  $r_{v_2,k}^{PLT}$  is obtained as the variance of the averaged prediction errors (as in (4.9)), the associated virtual noise  $n_{v_2,k}$  can be considered as zero mean with variance  $\sigma_{n_{v_2,k}}^2 = \text{Var}(r_{v_2,k}^{PLT})$ . Consequently, the variances of the virtual noises (i.e.  $\sigma_{n_{v_1,k}}^2$  and  $\sigma_{n_{v_2,k}}^2$ ) will be exploited as the weighting coefficients within the formulation of the two-step LS estimator.



## Chapter 5

# Formulation of the GPLT

## Algorithm

The geometric relationship between the MS and its associated BSs (i.e. indicated by the corresponding GDOP value) will affect the precision for location estimation and tracking. The concept of the proposed GPLT scheme is to adjust the positions of the designed virtual BSs such that the predicted MS will be situated at a location with a smaller GDOP value. The modified virtual BS's positions will therefore be adopted associated with the existing BSs for location estimation. Similarly, the two-BSs and the single-BS cases are considered as follows. First, we will explain the formulations of the GDOP shortly.

### 5.1 The Geometric Dilution of Precision (GDOP)

The GDOP [22] is defined as the ratio between the location estimation error and the associated measurement error. It is utilized as an index for observing the location precision of the MS under different geometric location within the networks (e.g. the cellular or the satellite networks). In general, a larger GDOP value corresponds to a comparably worse geometric layout (established by the MS and its associated BSs), which consequently results in augmented errors for location estimation. On the other hand, as the GDOP value becomes smaller, the effect from the geometric relationship to the location estimation accuracy will turn out to

be insignificant. Considering the MS's location under the two-dimensional coordinate, the GDOP value (G) obtained at the position  $\mathbf{x}_k$  can be represented as

$$\mathbf{G}_{\mathbf{x}_k} = \left\{ \text{trace} \left[ (\mathbf{H}_{\mathbf{x}_k}^T \mathbf{H}_{\mathbf{x}_k})^{-1} \right] \right\}^{\frac{1}{2}} \quad (5.1)$$

where

$$\mathbf{H}_{\mathbf{x}_k} = \begin{bmatrix} \frac{x_k - x_{1,k}}{\zeta_{1,k}} & \frac{y_k - y_{1,k}}{\zeta_{1,k}} \\ \dots & \dots \\ \frac{x_k - x_{i,k}}{\zeta_{i,k}} & \frac{y_k - y_{i,k}}{\zeta_{i,k}} \\ \dots & \dots \\ \frac{x_k - x_{N_k,k}}{\zeta_{N_k,k}} & \frac{y_k - y_{N_k,k}}{\zeta_{N_k,k}} \end{bmatrix} \quad (5.2)$$

It is noted that the elements within the matrix  $\mathbf{H}_{\mathbf{x}_k}$  can be acquired from (2.2). It has been shown in [22] that the minimum GDOP value frequently occurs around the center of the network layout, e.g. the minimum GDOP inside a  $K$ -side ( $K \geq 3$ ) regular polygon is shown to take place at the center of the layout and the value is obtained as  $G = \frac{2}{\sqrt{K}}$ . Moreover, the GDOP value and the Cramer-Rao Lower Bound (CRLB) are demonstrated to be identical given a Gaussian-distributed noise model [23].

## 5.2 The Two-BSs Case

In this case, the primary target for the GPLT scheme is to design the location of the virtual BS, i.e.  $\text{BS}_{v,1}$ :  $\mathbf{x}_{v_1,k}^{GPLT}$ . As shown in Fig. 4.1, two parameters (i.e. the distance  $r_{v_1,k}^{GPLT}$  and the angle  $\theta_k$ ) w.r.t. the predicted MS's position  $\hat{\mathbf{x}}_{k|k-1}$  are introduced to represent the designed virtual BS's position  $\mathbf{x}_{v_1,k}^{GPLT}$ . The selection of these two parameters within the GPLT algorithm is explained in the following subsections.

### 5.2.1 The Computation of the Angle $\theta_k$

The main objective of the GPLT scheme is to acquire the angle  $\theta_k$  of  $\mathbf{x}_{v_1,k}^{GPLT}$  such that the predicted MS ( $\hat{\mathbf{x}}_{k|k-1}$ ) will possess a minimal GDOP value within its network topology for location estimation. As illustrated in Fig. 4.1, the following equality can be obtained based on the geometric relationship:

$$\hat{\mathbf{x}}_{k|k-1} - \mathbf{x}_{v_1,k}^{GPLT} = (r_{v_1,k}^{GPLT} \cdot \cos \theta_k, r_{v_1,k}^{GPLT} \cdot \sin \theta_k) \quad (5.3)$$

As mentioned above, the position of the virtual BS ( $\mathbf{x}_{v_1,k}^{GPLT}$ ) is designed such that the predicted MS (i.e.  $\hat{\mathbf{x}}_{k|k-1}$ ) will be located at a minimal GDOP position based on the extended geometric set  $\mathbf{P}_{BS,k}^e = \{\mathbf{x}_{1,k}, \mathbf{x}_{2,k}, \mathbf{x}_{v_1,k}^{GPLT}\}$ . By incorporating (1) into (5.1) and (5.2), the GDOP value (i.e.  $G_{\hat{\mathbf{x}}_{k|k-1}}$ ) computed at the predicted MS's position  $\hat{\mathbf{x}}_{k|k-1} = (\hat{x}_{k|k-1}, \hat{y}_{k|k-1})$  can be obtained. The associated matrix  $\mathbf{H}_{\hat{\mathbf{x}}_{k|k-1}}$  becomes

$$\mathbf{H}_{\hat{\mathbf{x}}_{k|k-1}} = \begin{bmatrix} \frac{\hat{x}_{k|k-1} - x_{1,k}}{r_{1,k}} & \frac{\hat{y}_{k|k-1} - y_{1,k}}{r_{1,k}} \\ \frac{\hat{x}_{k|k-1} - x_{2,k}}{r_{2,k}} & \frac{\hat{y}_{k|k-1} - y_{2,k}}{r_{2,k}} \\ \frac{\hat{x}_{k|k-1} - x_{v_1,k}^{GPLT}}{r_{v_1,k}^{GPLT}} & \frac{\hat{y}_{k|k-1} - y_{v_1,k}^{GPLT}}{r_{v_1,k}^{GPLT}} \end{bmatrix} = \begin{bmatrix} \frac{\hat{x}_{k|k-1} - x_{1,k}}{r_{1,k}} & \frac{\hat{y}_{k|k-1} - y_{1,k}}{r_{1,k}} \\ \frac{\hat{x}_{k|k-1} - x_{2,k}}{r_{2,k}} & \frac{\hat{y}_{k|k-1} - y_{2,k}}{r_{2,k}} \\ \cos \theta_k & \sin \theta_k \end{bmatrix} \quad (5.4)$$

It is noted that the noiseless relative distance  $\zeta_{i,k}$  in (5.1) are approximately replaced by  $r_{i,k}$  in (5.4) since  $\zeta_{i,k}$  are considered unattainable. It can be observed from (5.4) that the matrix  $\mathbf{H}_{\hat{\mathbf{x}}_{k|k-1}}$  associated with the resulting  $G_{\hat{\mathbf{x}}_{k|k-1}}$  value are regarded as functions of the angle  $\theta_k$ , i.e.  $\mathbf{H}_{\hat{\mathbf{x}}_{k|k-1}}(\theta_k)$  and  $G_{\hat{\mathbf{x}}_{k|k-1}}(\theta_k)$ . Based on the objective of the GPLT scheme, the angle  $\theta_k^m$  which results in the minimal GDOP value can therefore be acquired as

$$\theta_k^m = \arg \left\{ \min_{\forall \theta_k} G_{\hat{\mathbf{x}}_{k|k-1}}(\theta_k) \right\} = \arg \left\{ \frac{\partial G_{\hat{\mathbf{x}}_{k|k-1}}(\theta_k)}{\partial \theta_k} = 0 \right\} \quad (5.5)$$

By substituting (5.4) and (5.1) into (5.5), the angle  $\theta_k^m$  can be computed as

$$\theta_k^m = \tan^{-1} \left( \frac{1 \pm \sqrt{1 + \Gamma^2}}{\Gamma} \right) \quad (5.6)$$



where

$$\Gamma = \frac{2[r_{2,k}^2(\hat{x}_{k|k-1} - x_{1,k})(\hat{y}_{k|k-1} - y_{1,k}) + r_{1,k}^2(\hat{x}_{k|k-1} - x_{2,k})(\hat{y}_{k|k-1} - y_{2,k})]}{r_{2,k}^2(\hat{x}_{k|k-1} - x_{1,k})^2 - r_{2,k}^2(\hat{y}_{k|k-1} - y_{1,k})^2 + r_{1,k}^2(\hat{x}_{k|k-1} - x_{2,k})^2 - r_{1,k}^2(\hat{y}_{k|k-1} - y_{2,k})^2} \quad (5.7)$$

It is noted that the noiseless relative distance  $\zeta_{i,k}$  in (5.7) are replaced by  $r_{i,k}$  for the computation of  $\Gamma$  since  $\zeta_{i,k}$  are in general considered unattainable. At each time instant  $k$ , the relative angle  $\theta_k^m$  between  $\hat{\mathbf{x}}_{k|k-1}$  and  $\mathbf{x}_{v_1,k}^{GPLT}$  can therefore be obtained such that  $\hat{\mathbf{x}}_{k|k-1}$  is located at the position with a minimal GDOP value based on its current network layout.

### 5.2.2 The Selection of the Distance $r_{v_1,k}^{GPLT}$

In this subsection, the virtual measurement  $r_{v_1,k}^{GPLT}$  will be determined, which can be utilized for acquiring the position of the virtual BS  $\mathbf{x}_{v_1,k}^{GPLT}$ . It is observed in (5.4) that the GDOP value at the predicted MS's position is primarily dominated by the relative angle (i.e.  $\theta_k$ ) between the MS and the BSs; while the distance information (i.e.  $r_{v_1,k}^{GPLT}$ ) is considered uninfluential to the GDOP value. This uncorrelated relationship between the GDOP value and the relative distance has also been observed as in [22]. The following Lemma shows that the selection of the distance  $r_{v_1,k}^{GPLT}$  becomes insignificant for the WLS-based location estimation.

**Lemma 1** *A time-based location estimation problem is considered for the MS using the Weighted Least Square (WLS) algorithm. Assuming that a measurement input from a specific BS is associated with zero mean random noises, the expected value of the location estimation error is independent to the distance between the specific BS and the MS.*

*Proof:* Considering three TOA measurements are available for estimating the MS's position (as described in (2.1) with  $N_k = 3$ ), it is assumed that the third TOA measurement  $r_{3,k}$  is only contaminated with random noises with zero mean value, i.e.  $E[n_{3,k}] = 0$  and  $e_{3,k} = 0$  in (2.1). The target of this proof is to illustrate that the expected value of the estimation error resulting from the WLS method is independent to the magnitude of the measurement input  $r_{3,k}$ . By combining (2.1) and (2.2), the following matrix format can be obtained:

$$\mathbf{A}_k \mathbf{b}_k = \mathbf{J}_k \quad (5.8)$$

where

$$\mathbf{b}_k = \begin{bmatrix} x_k & y_k & \beta_k \end{bmatrix}^T$$

$$\mathbf{A}_k = \begin{bmatrix} -2x_{1,k} & -2y_{1,k} & 1 \\ -2x_{2,k} & -2y_{2,k} & 1 \\ -2x_{3,k} & -2y_{3,k} & 1 \end{bmatrix} \quad \mathbf{J}_k = \begin{bmatrix} r_{1,k}^2 - \kappa_{1,k} \\ r_{2,k}^2 - \kappa_{2,k} \\ r_{3,k}^2 - \kappa_{3,k} \end{bmatrix}$$

It is noted that  $\beta_k = x_k^2 + y_k^2$  and  $\kappa_{i,k} = x_{i,k}^2 + y_{i,k}^2$  for  $i = 1, 2$ , and  $3$ . Based on (5.8), the MS's estimated position by adopting the WLS method (i.e.  $\hat{\mathbf{x}}_k = [\hat{x}_k, \hat{y}_k]^T$ ) can be acquired as

$$\hat{\mathbf{x}}_k = \mathbf{C}(\mathbf{A}_k^T \boldsymbol{\Psi}^{-1} \mathbf{A}_k)^{-1} \mathbf{A}_k^T \boldsymbol{\Psi}^{-1} \mathbf{J}_k \quad (5.9)$$

where

$$\mathbf{C} = \begin{bmatrix} 1 & 0 & 0 \\ 0 & 1 & 0 \end{bmatrix} \quad (5.10)$$

$$\boldsymbol{\Psi} = E[\psi\psi^T] = E[(\mathbf{J}_k - \mathbf{A}_k \mathbf{b}_k)(\mathbf{J}_k - \mathbf{A}_k \mathbf{b}_k)^T] = 4c^2 \mathbf{B} \mathbf{L} \mathbf{B} \quad (5.11)$$

The parameter  $\boldsymbol{\Psi}$  is denoted as the error covariance matrix where  $\mathbf{B} = \text{diag}\{\zeta_{1,k}, \zeta_{2,k}, \zeta_{3,k}\}$ .  $\mathbf{L}$  represents the covariance matrix of measured noise. The primary concern of this proof is to acquire the expected value of the estimation error  $\Delta \hat{\mathbf{x}}_k = [\Delta \hat{x}_k, \Delta \hat{y}_k]^T$ , which can be obtained by rewriting (5.9) as

$$\Delta \hat{\mathbf{x}}_k = \mathbf{C}(\mathbf{A}_k^T \boldsymbol{\Psi}^{-1} \mathbf{A}_k)^{-1} \mathbf{A}_k^T \boldsymbol{\Psi}^{-1} \Delta \mathbf{J}_k \quad (5.12)$$

It is noted that (5.12) indicates that the estimation error vector  $\Delta \hat{\mathbf{x}}_k$  is incurred by the variation within the vector  $\mathbf{J}_k$ . The value of  $\Delta \mathbf{J}_k$  is obtained by considering the variations

from the measurement inputs as (i.e.  $r_{i,k} = \zeta_{i,k} + n_{i,k} + e_{i,k}$  in (2.1))

$$\Delta \mathbf{J}_k = \begin{bmatrix} 2\zeta_{1,k}(n_{1,k} + e_{1,k}) + (n_{1,k} + e_{1,k})^2 \\ 2\zeta_{2,k}(n_{2,k} + e_{2,k}) + (n_{2,k} + e_{2,k})^2 \\ 2\zeta_{3,k}n_{3,k} + n_{3,k}^2 \end{bmatrix} \simeq \begin{bmatrix} 2\zeta_{1,k}(n_{1,k} + e_{1,k}) \\ 2\zeta_{2,k}(n_{2,k} + e_{2,k}) \\ 2\zeta_{3,k}n_{3,k} \end{bmatrix} \quad (5.13)$$

where  $e_{3,k}$  is considered zero as mentioned at the beginning of this proof. The approximation is valid by considering that the noiseless distance  $\zeta_{i,k}$  is in general larger than the combined noise effect ( $n_{i,k} + e_{i,k}$ ). For simplicity and without lose of generality, coordinate transformation can be adopted within (5.12) such that  $(x_{1,k}, y_{1,k}) = (0, 0)$ . The expected value of the estimation error (i.e.  $\Delta \hat{\mathbf{x}}_k = [\Delta \hat{x}_k, \Delta \hat{y}_k]^T$ ) can therefore be acquired by expanding (5.12) as

$$\begin{aligned} E[\Delta \hat{x}_k] &= E \left[ \frac{\zeta_{1,k}(n_{1,k} + e_{1,k})(y_{2,k} - y_{3,k}) + \zeta_{2,k}(n_{2,k} + e_{2,k})y_{3,k} - \zeta_{3,k}n_{3,k}y_{2,k}}{x_{3,k}y_{2,k} - x_{2,k}y_{3,k}} \right] \\ &= E \left[ \frac{\zeta_{1,k}(n_{1,k} + e_{1,k})(y_{2,k} - y_{3,k}) + \zeta_{2,k}(n_{2,k} + e_{2,k})y_{3,k}}{x_{3,k}y_{2,k} - x_{2,k}y_{3,k}} \right] \end{aligned} \quad (5.14)$$

$$\begin{aligned} E[\Delta \hat{y}_k] &= E \left[ \frac{\zeta_{1,k}(n_{1,k} + e_{1,k})(x_{2,k} - x_{3,k}) + \zeta_{2,k}(n_{2,k} + e_{2,k})x_{3,k} - \zeta_{3,k}n_{3,k}x_{2,k}}{y_{3,k}x_{2,k} - y_{2,k}x_{3,k}} \right] \\ &= E \left[ \frac{\zeta_{1,k}(n_{1,k} + e_{1,k})(x_{2,k} - x_{3,k}) + \zeta_{2,k}(n_{2,k} + e_{2,k})x_{3,k}}{y_{3,k}x_{2,k} - y_{2,k}x_{3,k}} \right] \end{aligned} \quad (5.15)$$

It is noted that the second equalities for both (5.14) and (5.15) are attained based on the assumption that  $E[n_{3,k}] = 0$ . From (5.14) and (5.15), it can clearly be observed that the expected value of the estimation error (i.e.  $E[\Delta \hat{\mathbf{x}}_k] = [E[\Delta \hat{x}_k], E[\Delta \hat{y}_k]]^T$ ) is independent to the measured distance  $r_{3,k}$  under the assumption that its associated measurement noise  $n_{3,k}$  is considered a zero mean random variable, i.e.  $E[r_{3,k}] = E[\zeta_{3,k}] + E[n_{3,k}] = E[\zeta_{3,k}]$ . This completes the proof.

This lemma states that the expected value of the location estimation error is independent to the distance between a specific BS to the MS if the noises associated with the measurement inputs are statistically distributed with a zero mean value. In generic time-based location estimation, the phenomenon stated in Lemma 1 does not usually exist since most of the measurement inputs are contaminated with NLOS noises, i.e.  $e_{i,k}$  in (2.1) is randomly distributed

with positive mean value. The NLOS error is augmented as the distance between the specific BS and the MS is increased, which causes the corresponding measurement input to become unreliable comparing with the other signal sources. This result is consistent with the intuition that BSs with closer distances to the MS are always selected for location estimation. In the proposed GPLT scheme, the virtual measurement  $r_{v_1,k}^{GPLT}$  is considered as a designed distance which is infected by its corresponding zero mean virtual noise  $n_{v_1,k}$  as in (4.10). Based on Lemma 1, the selection of the distance  $r_{v_1,k}^{GPLT}$  becomes uninfluential to the estimation error while exploiting the WLS algorithm for location estimation. This result is similar to the derived GDOP value that is unrelated to the distance information between the BSs and the MS (as can be observed from (5.4)). In the simulation section, the uncorrelated relationship between  $r_{v_1,k}^{GPLT}$  and the estimation error will further be validated by exploiting the two-step LS estimator, which is considered one of the the WLS-based algorithms for location estimation. It will be demonstrated via the simulation results that the influence from the length of the virtual measurement to the estimation error is considered insignificant.

The procedures of the proposed GPLT scheme under the two-BSs case is explained as follows. The target is to obtain the position of the MS at the  $k^{th}$  time step (i.e.  $\hat{\mathbf{x}}_{k|k}$ ) based on the available information, including the measurement and location information acquired from both BS<sub>1</sub> and BS<sub>2</sub> along with the predicted position of the MS (i.e.  $\hat{\mathbf{x}}_{k|k-1}$ ). Two steps are involved within the proposed GPLT scheme: (i) the determination of the virtual BS's position and the virtual measurement; and (ii) the estimation and tracking of the MS's position. As shown in Fig. 4.1, the orientation of the virtual BS ( $\theta_k^m$ ) relative to the the predicted MS's position  $\hat{\mathbf{x}}_{k|k-1}$  is determined based on the criterion of minimizing the GDOP value on  $\hat{\mathbf{x}}_{k|k-1}$  (as obtained from (5.5) and (5.6)). As was indicated by Lemma 1 in Subsection V.A.(2), the selection of the virtual distance  $r_{v_1,k}^{GPLT}$  w.r.t. the predicted MS's position  $\hat{\mathbf{x}}_{k|k-1}$  is considered insignificant to the estimation errors. Therefore, the distance is selected the same value as was designed in the PLT algorithm, i.e.  $r_{v_1,k}^{GPLT} = r_{v_1,k}^{PLT}$  as in (4.5). The location of the virtual BS ( $\mathbf{x}_{v_1,k}^{GPLT}$ ) and the length of the virtual measurement ( $r_{v_1,k}^{GPLT}$ ) can consequently be acquired. It is also noticed that the design of the virtual noise can therefore be selected

the same as that in the PLT scheme, i.e. zero mean random distributed with variance  $\sigma_{n_{v_1,k}}^2 = \text{Var}(r_{v_1,k}^{PLT}) = \text{Var}(\|\hat{\mathbf{x}}_{k|k-1} - \hat{\mathbf{x}}_{k-1|k-1}\|)$ .

After acquiring the information of the virtual BS as the additional signal source, the extended sets of the BSs and the measurement inputs can be established as  $\mathbf{P}_{BS,k}^e = \{\mathbf{x}_{1,k}, \mathbf{x}_{2,k}, \mathbf{x}_{v_1,k}^{GPLT}\}$  and  $\mathbf{r}_k^e = \{r_{1,k}, r_{2,k}, r_{v_1,k}^{GPLT}\}$ . As illustrated in Fig. 3.3, the extended set of signal sources are utilized as the inputs to the two-step LS estimator. The estimated MS's position  $\hat{\mathbf{x}}_{k|k}$  can therefore be obtained by adopting the correcting phase of the Kalman filter, which completes the location estimation and tracking processes at the  $k^{th}$  time step.

### 5.3 The Single-BS Case

As illustrated in Fig. 4.2, only one BS ( $\mathbf{x}_{1,k}$ ) associated with the measurement input  $r_{1,k}$  is available at the considered  $k^{th}$  time instant. Additional two virtual BSs associated with their virtual measurements are required as the inputs for the two-step LS estimator, i.e.  $\mathbf{P}_{BS_v,k}^{GPLT} = \{\mathbf{x}_{v_1,k}^{GPLT}, \mathbf{x}_{v_2,k}^{GPLT}\}$  and  $\mathbf{r}_{v,k}^{GPLT} = \{r_{v_1,k}^{GPLT}, r_{v_2,k}^{GPLT}\}$ . By adopting the design from the PLT scheme with the single-BS case, the first virtual BS is designed to be located at  $\mathbf{x}_{v_1,k}^{GPLT} = \hat{\mathbf{x}}_{k-1|k-1}$  associated with the first virtual measurement  $r_{v_1,k}^{GPLT}$  as defined in (4.5).

The second virtual measurement  $r_{v_2,k}^{GPLT}$  is also designed to be the same as in the PLT scheme (in (4.9)), which considers the averaged prediction error from the previous time steps. As shown in Fig. 4.2, the position of the second virtual BS ( $\mathbf{x}_{v_2,k}^{GPLT}$ ) is designed at a location with distance  $r_{v_2,k}^{GPLT}$  relative to the predicted MS's position  $\hat{\mathbf{x}}_{k|k-1}$ . The relative angle  $\theta_k^m$  between  $\mathbf{x}_{v_2,k}^{GPLT}$  and  $\hat{\mathbf{x}}_{k|k-1}$  is determined by minimizing the GDOP value based on the predicted MS's position  $\hat{\mathbf{x}}_{k|k-1}$ . Both of the information from BS<sub>1</sub> and BS<sub>v<sub>1</sub></sub> alone with the predicted MS's position  $\hat{\mathbf{x}}_{k|k-1}$  are utilized for the computation of the angle  $\theta_k^m$  (as in (5.5) and (5.6)). It is noticed that instead of altering the position of BS<sub>v<sub>1</sub></sub>, the BS<sub>v<sub>2</sub></sub>'s location is adjusted in order to acquire a better GDOP value for the predicted MS  $\hat{\mathbf{x}}_{k|k-1}$ . The design concept is primarily owing to the fact that the average prediction error is in general smaller than the length of each prediction within the Kalman filtering formulation, i.e.  $r_{v_1,k}^{GPLT} > r_{v_2,k}^{GPLT}$ . The expected MS's position  $\hat{\mathbf{x}}_{k|k-1}$  is considered more sensitive to  $r_{v_2,k}^{GPLT}$  due to its smaller value comparing

with  $r_{1,k}$  and  $r_{v_1,k}^{GPLT}$ . It will be beneficial to adjust the location of  $BS_{v_2}$  (by rotating the angle  $\theta_k^m$ ) such that a smaller GDOP value can be achieved at the predicted location of the MS ( $\hat{\mathbf{x}}_{k|k-1}$ ).

As indicated by Lemma 1, the selection of the virtual measurement  $r_{v_2,k}^{GPLT}$  is considered insignificant on the precision for location estimation. Nevertheless, the distance  $r_{v_2,k}^{GPLT}$  is chosen as in (4.9) in order to facilitate the design of the weighting coefficient associated with the two-step LS estimator. Similar to the design within the PLT scheme, the virtual noise associated with the second virtual measurement  $r_{v_2,k}^{GPLT}$  can be regarded as zero mean with variance  $\sigma_{n_{v_2,k}}^2 = \text{Var}(r_{v_2,k}^{GPLT})$ . Therefore, the information from the additional two virtual measurements  $r_{v_1,k}^{GPLT}$  and  $r_{v_2,k}^{GPLT}$  can be acquired such as to provide sufficient signal sources for the two-step LS location estimator. The precision for location estimation and tracking of the MS can consequently be enhanced.



## Chapter 6

# Performance Evaluation

Simulations are performed to show the effectiveness of the proposed PLT and GPLT schemes under different numbers of BSs, including the scenarios with deficient signal sources. The noise models and the simulation parameters are illustrated in Subsection A. Subsection B validates the GPLT scheme according to the variations from the relative angle and the distance between the MS and the designed virtual BS. The performance comparison between the proposed PLT and GPLT algorithms with the other existing location tracking schemes, i.e. the Kalman Tracking (KT) and the Cascade Location Tracking (CLT) techniques, are conducted in Subsection C.

### 6.1 The Noise Models and the Simulation Parameters

Different noise models [28] [47] for the the TOA measurements are considered in the simulations. The model for the measurement noise of the TOA signals is selected as the Gaussian distribution with zero mean and 10 meters of standard deviation, i.e.  $n_{i,k} \sim \mathcal{N}(0, 100)$ . On the other hand, an exponential distribution  $p_{e_{i,k}}(\tau)$  is assumed for the NLOS noise model of the TOA measurements as

$$p_{e_{i,k}}(v) = \begin{cases} \frac{1}{\lambda_{i,k}} \exp\left(-\frac{v}{\lambda_{i,k}}\right) & v > 0 \\ 0 & \text{otherwise} \end{cases} \quad (6.1)$$

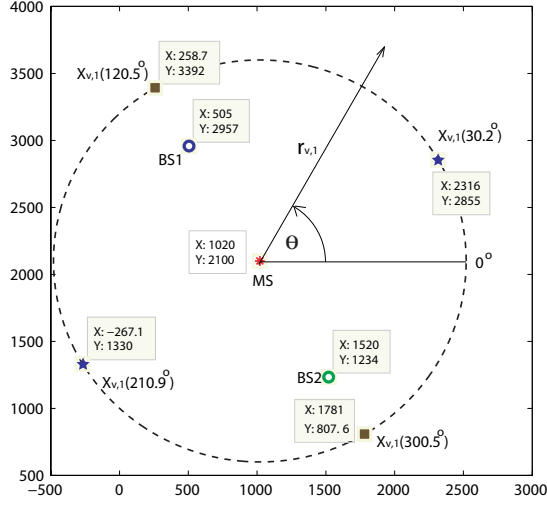


Figure 6.1: An Exemplify Diagram for the Scenarios with the Two-BSs Layout. Stars ( $\mathbf{x}_{v,1}(30.2^\circ)$  and  $\mathbf{x}_{v,1}(210.9^\circ)$ ): the Positions of the Virtual BS Cause the Minimal GDOP Value of the MS; Squares ( $\mathbf{x}_{v,1}(120.5^\circ)$  and  $\mathbf{x}_{v,1}(300.5^\circ)$ ): the Positions of the Virtual BS Cause the Maximal GDOP Value of the MS

where  $\lambda_{i,k} = c \cdot \tau_{i,k} = c \cdot \tau_m (\zeta_{i,k})^\varepsilon \rho$ . The parameter  $\tau_{i,k}$  is the RMS delay spread between the  $i^{th}$  BS to the MS.  $\tau_m$  represents the median value of  $\tau_{i,k}$ , which is selected as 0.1 in the simulations.  $\varepsilon$  is the path loss exponent which is assumed to be 0.5, and the factor for shadow fading  $\rho$  is set to 1 in the simulations. The parameters for the noise models as listed in this subsection primarily fulfill the environment while the MS is located within the rural area. It is noticed that the reason for selecting the rural area as the simulation scenario is due to its higher probability to suffer from deficiency of signal sources. Moreover, the sampling time  $\Delta t$  is chosen as 1 sec in the simulations.

## 6.2 Validation of the GPLT Scheme

### 6.2.1 Validation with Angle Effect

As mentioned in Subsection V.A.(1), the primary objective of the proposed GPLT algorithm is to adjust the position of the virtual BS such that the predicted MS can be situated at a location



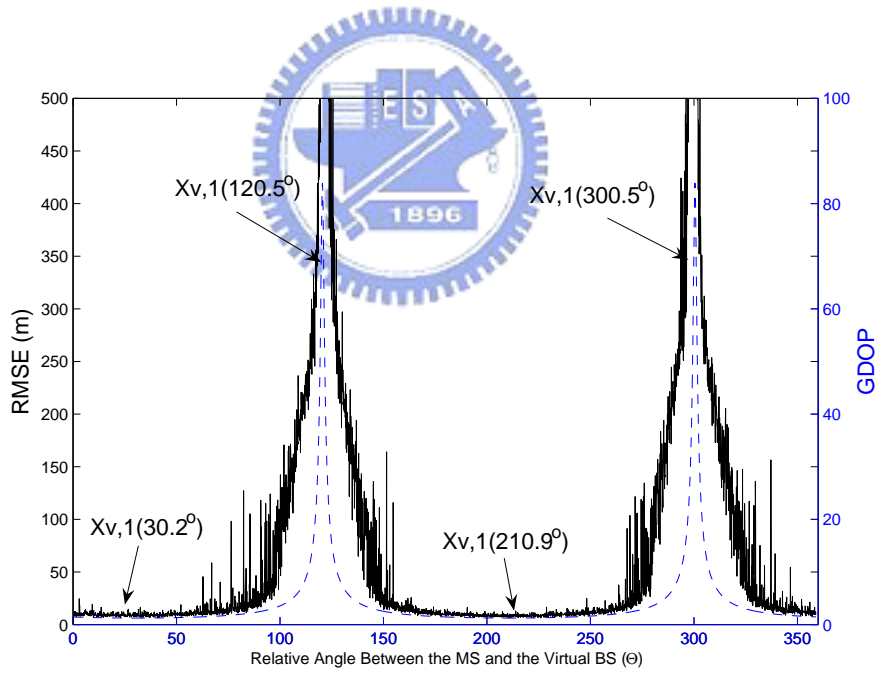
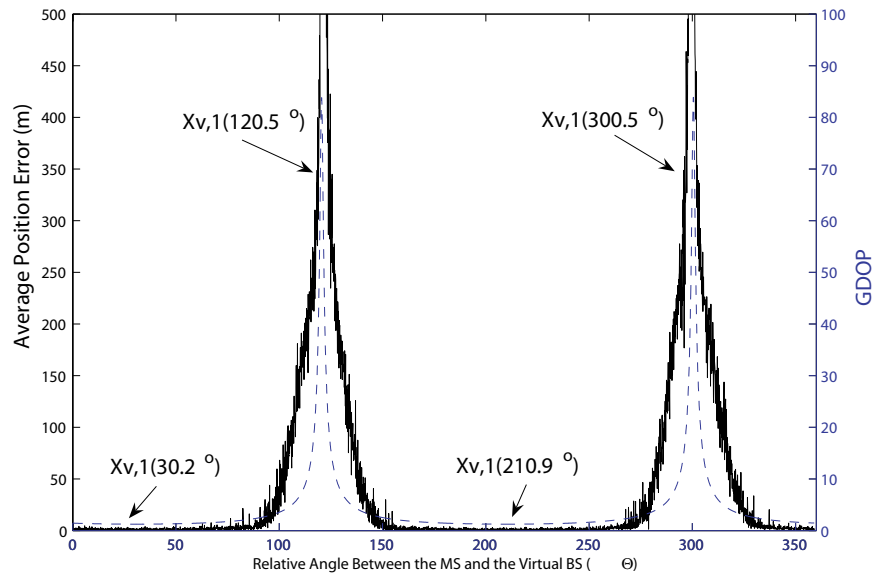


Figure 6.2: Top Plot: the Average Position Error (Solid Line) and the GDOP Value (Dashed Line) vs the Relative Angle Between the MS and the Virtual BS ( $\theta$ ); Bottom Plot: the RMSE (Solid Line) and the GDOP Value (Dashed Line) vs the Relative Angle Between the MS and the Virtual BS ( $\theta$ )

with minimal GDOP value. The design concept implicitly indicates that the estimation error can be reduced if the MS is possessed with a smaller GDOP value formed by its geometric layout. In this subsection, the relationship between the estimation errors and the GDOP values will be verified via simulations. As shown in Fig. 6.1, the two-BS case is considered associated with the locations of the BSs are  $\text{BS}_1 = (505, 2957)$  and  $\text{BS}_2 = (1520, 1234)$  in meters. The MS's true position is located at  $\mathbf{x} = (1020, 2100)$  m. The position of the virtual BS is assumed at  $\mathbf{x}_{v,1}(\theta) = (1020 + 1500 \cos \theta, 2100 + 1500 \sin \theta)$  m with  $\theta = 0 \sim 359^\circ$ . It can be seen that the potential positions of the virtual BS are considered to be located at a distance 1500 meters away from the MS's true position along with different relative angles  $\theta$ .

Fig. 6.2 illustrates the comparison between the average position error (left plot), the RMSE (right plot), and the GDOP value versus the relative angle ( $\theta$ ) between the true MS and the virtual BS. It is noted that the Average Position Error ( $\Delta x$ ) and the RMSE are computed as:  $\Delta x = \left[ \sum_{i=1}^N \|\mathbf{x} - \hat{\mathbf{x}}(i)\| \right] / N$  and  $\text{RMSE} = \left[ \sum_{i=1}^N \|\mathbf{x} - \hat{\mathbf{x}}(i)\|^2 / N \right]^{1/2}$  where  $N = 50$  indicates the number of simulation runs. It is also noticed that the GDOP value ( $G_{\mathbf{x}}$ ) is evaluated at the MS's true position; while the estimated MS's position  $\hat{\mathbf{x}}(i)$  is obtained by the two-step LS estimator employing the various positions of the virtual BS, i.e.  $\mathbf{x}_{v,1}(\theta)$  for  $\theta = 0 \sim 359^\circ$ . It can be observed from both plots in Fig. 6.2 that the average position error and the RMSE follow the similar trend as the computed GDOP value. Both the minimal mean estimation error (associated with the RMSE) and the minimal GDOP value occur at the locations of  $\mathbf{x}_{v,1}(30.2^\circ) = (2316, 2855)$  m and  $\mathbf{x}_{v,1}(210.9^\circ) = (-267.1, 1330)$  m. It is noted that the angle  $\theta_k^m$  for the minimal GDOP value can also be directly computed and verified from (5.6). Moreover, the maximal GDOP values and the maximal estimation errors (including both the average position error and the RMSE) happen around the locations of  $\mathbf{x}_{v,1}(120.5^\circ) = (258.7, 3392)$  m and  $\mathbf{x}_{v,1}(300.5^\circ) = (1781, 807.6)$  m. The results can further be validated by observing the geometric layout as in Fig. 6.2. The minimal GDOP values of the true MS occur as the three BSs form an equilateral triangle; while the maximal GDOP values happen as the three BSs are situated along a straight line. The above observations validate the effectiveness of the proposed GPLT scheme by obtaining a position of the virtual BS with a

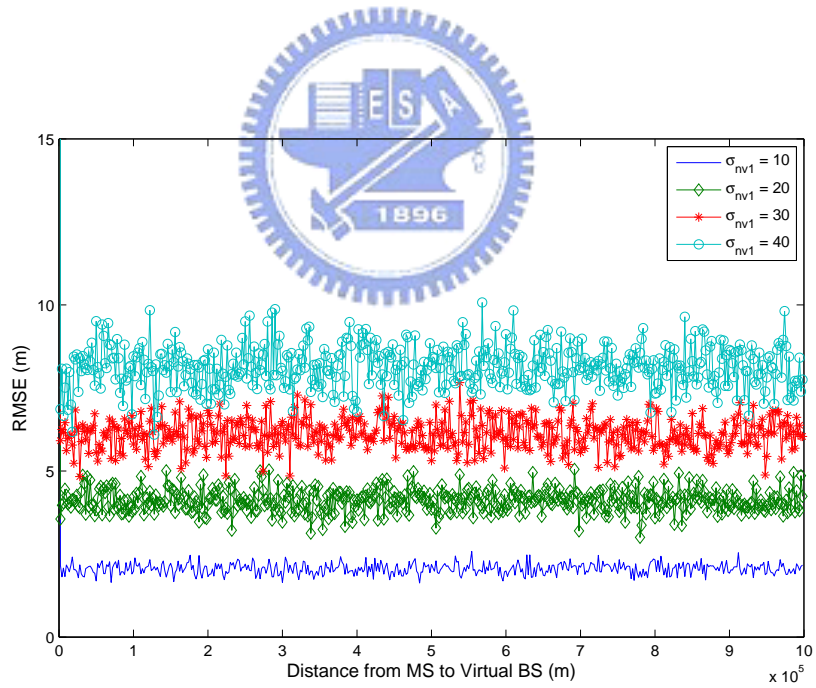
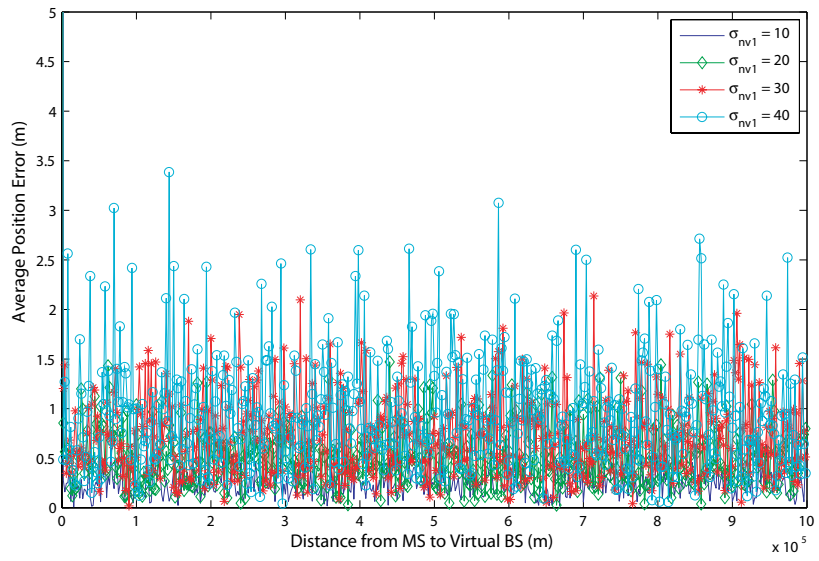


Figure 6.3: Top Plot: the Average Position Errors vs the Relative Distance Between the MS and the Virtual BS ( $r_{v,1}$ ); Bottom Plot: the RMSE vs the Relative Distance Between the MS and the Virtual BS ( $r_{v,1}$ ) (with  $\sigma_{n_{v,1}} = 10, 20, 30, 40$ )

smaller GDOP value, which consequently reduces the corresponding estimation error. On the other hand, the estimation errors can be severely augmented if the MS happens to be located at a position with the maximum GDOP value by adopting other schemes. It can therefore be concluded that the results obtained from the simulations comply with the design objectives of the GPLT algorithm.

### 6.2.2 Validation with Distance Effect

In this subsection, the results obtained from Lemma 1 will be validated via simulations. It is stated in Lemma 1 that the expected value of the estimation error is independent to the distance between the MS and a specific BS by adopting the WLS location estimation algorithm. In order to validate Lemma 1 by the simulation data, the estimation errors induced by adopting the two-step LS estimator will be obtained for the evaluation of the distance effect. Fig. 6.3 illustrates the average position error (left plot) and the RMSE (right plot) acquired from the two-step LS method under different relative distances between the MS and the virtual BS (i.e.  $r_{v,1}$ ). It is noted that the distance  $r_{v,1}$  is simulated from 1 to  $10^6$  m along the angle  $\theta = 60^\circ$  as shown in Fig. 6.1. The four simulated results are conducted under different signal variations (i.e.  $\sigma_{n_{v_1}} = 10, 20, 30, 40$ ) in order to exam the potential effect from the signal variances. As can be expected, the estimation errors are observed to be independent to the relative distance between the MS and the virtual BS, which are similar to the results as concluded from Lemma 1. Moreover, it is also reasonable to perceive that the increases on the signal variances  $\sigma_{n_{v_1}}$  will induce proportional augmentation on the RMSE (in the right plot of Fig. 6.3); while the average position error is considered not related to the changes due to the signal variations (in the left plot of Fig. 6.3). From the above observations via the simulation data, the uncorrelated relationship between the distance  $r_{v,1}$  and the estimation error is found to be consistent with the results as acquired from Lemma 1.

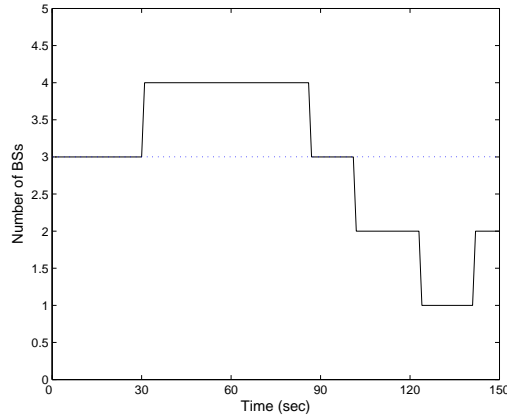


Figure 6.4: Total Number of Available BSs ( $N_k$ ) vs. Simulation Time (sec)

### 6.3 Simulation Results

The performance comparisons between the KT scheme, the CLT scheme, and the proposed PLT and GPLT algorithms are conducted under the rural environment. Fig. 6.4 illustrates the scenarios with various numbers of BSs (i.e. the  $N_k$  values) that are available at different time instants. It can be seen that the number of BSs becomes insufficient (i.e.  $N_k < 3$ ) from the time interval of  $t = 102$  to 150 sec. The total simulation interval is set as 150 seconds.

Figs. 6.5 to 6.7 illustrate the performance comparisons of the trajectory, the velocity, and the acceleration tracking using the four algorithms. The estimated trajectories obtained from these schemes are illustrated via the solid lines; while the true trajectories are denoted by the dashed lines. The locations of the BSs are represented by the red empty circles as in Fig. 6.5. The acceleration is designed to vary at time  $t = 40, 55,$  and  $120$  sec from  $\mathbf{a}_k = (a_{x,k}, a_{y,k}) = (0.5, 0), (-1, 1), (0, 0)$  to  $(0.2, -0.5)$  m/sec<sup>2</sup> (as shown in Fig. 6.7). It is noted that the number of BSs becomes insufficient during the second acceleration change (i.e. at  $t = 102$  sec). By observing the starting time interval between  $t = 0$  and 101 sec (where the number of BSs is sufficient), the four algorithms provide similar performance on location tracking as shown in the  $x$ - $y$  plots in Fig. 6.5. As illustrated in Figs. 6.6 and 6.7, it can be seen that the KT scheme can provide better performance on the velocity and acceleration tracking during the transient phase (i.e from  $t = 0$  to 10 sec). The reason is attributed to its compromise

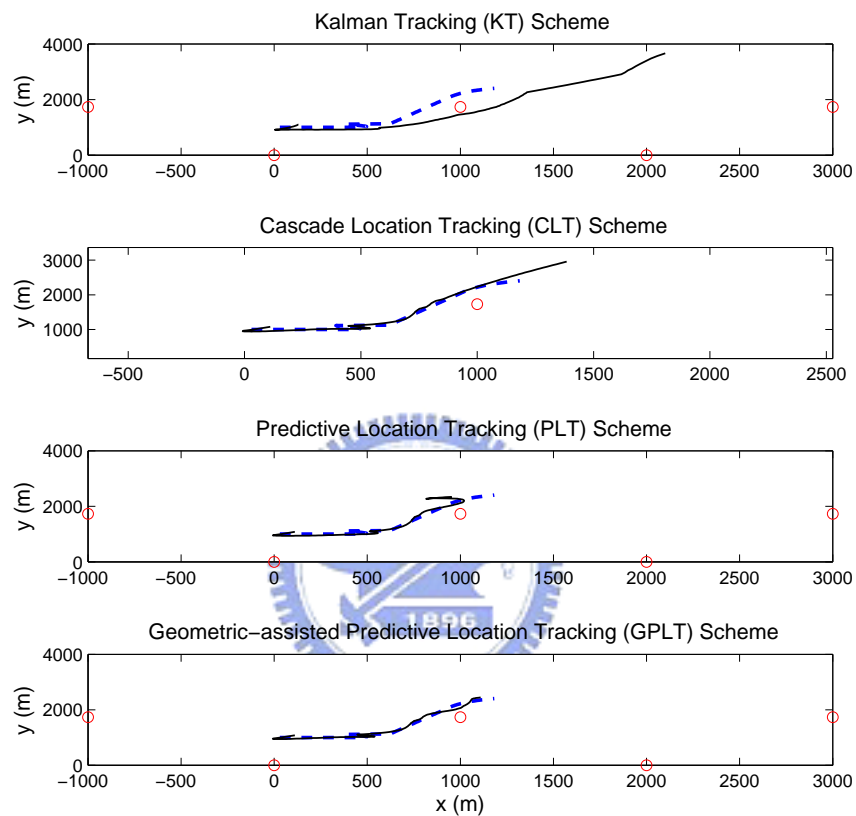


Figure 6.5: Trajectory Tracking of the MS Using the KT (Top Plot), the CLT (2<sup>nd</sup> Plot), the PLT (3<sup>rd</sup> Plot), and the GPLT (Bottom Plot) Schemes (Solid Lines: Estimated Trajectories; Dashed Lines: True Trajectories; Red Empty Circles: the Position of the BSs)

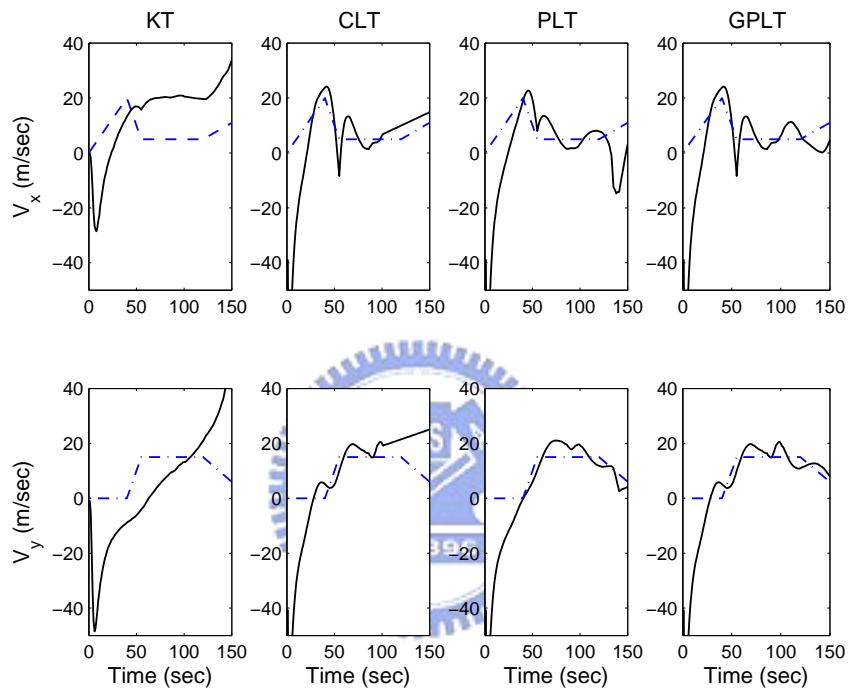


Figure 6.6: Velocity Tracking of the MS Using the KT (Left Plots), the CLT (Middle-Left Plots), the PLT (Middle-Right Plots), and the GPLT (Right Plots) Schemes (Solid Lines: Estimated Trajectories; Dashed Lines: True Trajectories)

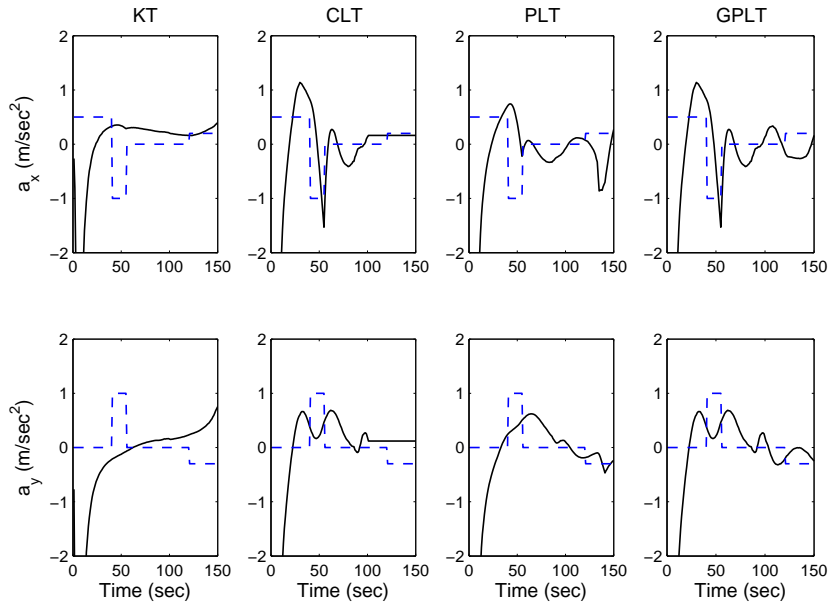


Figure 6.7: Acceleration Tracking of the MS Using the KT (Left Plots), the CLT (Middle-Left Plots), the PLT (Middle-Right Plots), and the GPLT (Right Plots) Schemes (Solid Lines: Estimated Trajectories; Dashed Lines: True Trajectories)

between the estimated state variables,  $\hat{\mathbf{x}}_k$ ,  $\hat{\mathbf{v}}_k$ , and  $\hat{\mathbf{a}}_k$ . However, the KT scheme results in the worst performance between the four schemes after the transient phase (as shown in Figs. 6.6 and 6.7). Owing to the utilization of an external location estimator within the KT scheme, the estimation errors are increasingly accumulated caused by the potential inaccuracy of the estimator.

During the time interval between  $t = 102$  and  $150$  sec with inadequate signal sources, it can be observed that only the proposed GPLT scheme can achieve satisfactory performance in the trajectory, the velocity, and the acceleration tracking. The estimated trajectories obtained from both the KT and the CLT schemes diverge from the true trajectories due to the inadequate number of measurement inputs. It is noticed that the inaccuracy within the PLT scheme is primarily resulted from the implicitly worse geometric layout at certain time instants, which will further be explained by the GDOP plot as in Fig. 6.10.

Moreover, Figs. 6.8 and 6.9 illustrate the average position error and the RMSE (i.e. characterizing the signal variances) for location estimation and tracking of the MS. The four



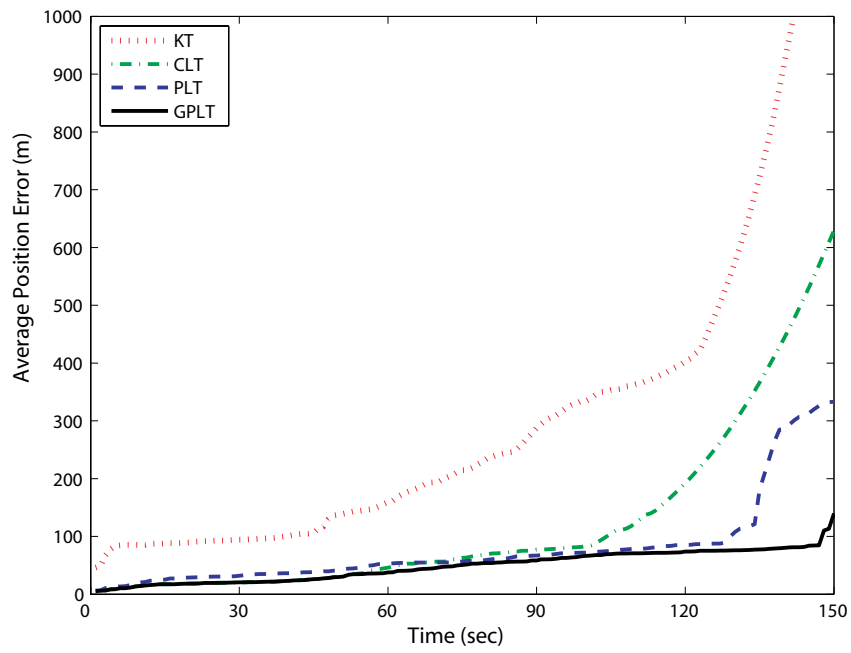


Figure 6.8: Performance Comparison: Average Position Error vs. Simulation Time (sec)

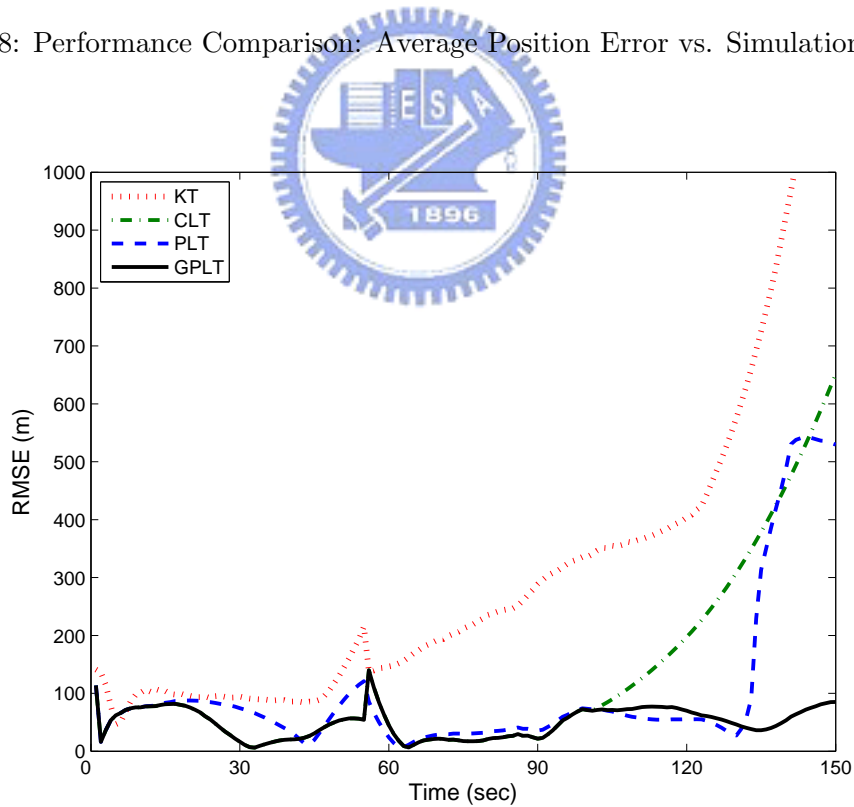


Figure 6.9: Performance Comparison: RMSE vs. Simulation Time (sec)

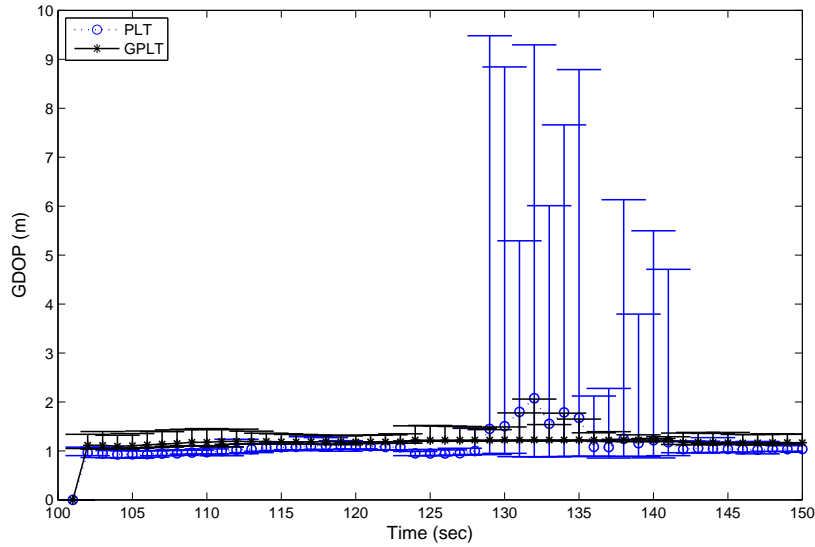


Figure 6.10: Comparison of the Mean GDOP Values (Associated with Their Confident Intervals) Between the PLT and the GPLT schemes During the Time Interval with Deficient Signal Sources

location tracking schemes are compared based on the same simulation scenario as shown in Fig. 6.4. It can be observed from both plots that the proposed GPLT and PLT algorithms outperform the conventional KT and CLT schemes. During the time interval of 40 to 55 sec while the acceleration changes, the RMSEs obtained from these four schemes slightly deviate for the acceleration adjustment. The main differences between these algorithms occur while the signal sources become insufficient after the time instant of  $t = 102$  sec. The proposed GPLT scheme can still provide consistent location estimation and tracking; while the other three algorithms result in augmented estimation errors. The major reason is attributed to the assisted information that is fed back into the location estimator while the signal sources are deficient. Furthermore, the GPLT algorithm outperforms the PLT scheme (especially under the situations with the number of BSs equal to 1) primarily due to its exploitation of the GDOP criterion.

The comparison of the mean GDOP values (associated with their confident intervals) between the PLT and the GPLT schemes is illustrated in Fig. 6.10. It is noted that the averaged GDOP values are computed based on 25 simulation runs. The mean GDOP values

are compared only during the time interval with deficient signal sources, i.e. while the virtual BSs and the virtual measurements are exploited in both schemes. It can be observed that the GDOP values obtained from the GPLT algorithm are consistent during the simulation period with reasonable variations. On the other hand, the GDOP values acquired from the PLT scheme result in larger variations, especially during the time interval of  $t = 129$  to  $141$  sec. The results are consistent with those estimation errors as acquired from Figs. 6.8 and 6.9 that worse GDOP value will result in incorrect location estimation of the MS. During the time interval of  $t = 102$  to  $128$  sec, the GDOP values obtained from both schemes are considered similar, which represent that comparable geometric topology are formed by their individual virtual BSs. The geometric effect will not be an influential factor to the estimation error for the MS. On the other hand, during the time interval of  $t = 129$  to  $141$  sec, sudden deviates in the GDOP values are observed by using the PLT scheme. The larger average position error and the RMSE within the PLT algorithm (as seen from Figs. 6.8 and 6.9 at around  $t = 135$  sec) can therefore be attributed to the corresponding increased GDOP values and variations. Nevertheless, with the adoption of the minimal GDOP criterion, the proposed GPLT scheme can still maintain consistent GDOP values under different numbers of available signal inputs. The resulting estimation error and RMSE can consequently be controlled within a reliable interval. The effectiveness of the GPLT algorithm is therefore perceived, especially under insufficient signal sources (i.e.  $N_k = 1$  and  $2$ ).

## Chapter 7

# Conclusion

In this paper, the Predictive Location Tracking (PLT) and the Geometric-assisted Predictive Location Tracking (GPLT) schemes are proposed. The predictive information obtained from the Kalman filtering formulation is exploited as the additional measurement inputs for the location estimator. With the feedback information, sufficient signal sources become available for location estimation and tracking of a MS. Moreover, the GPLT algorithm adjusts the locations of its virtual Base Stations based on the GDOP criterion. It is shown in the simulation results that the proposed GPLT algorithm can provide consistent accuracy for location estimation and tracking even under the environments with insufficient signal sources.

# Bibliography

- [1] "Revision of the Commissions Rules to Insure Compatibility with Enhanced 911 Emergency Calling Systems," *Federal Communications Commission*, 1996.
- [2] N. Patwari, J. N. Ash, S. Kyperountas, A. O. Hero III, R. L. Moses, and N. S. Correal, "Locating the Nodes: Cooperative Localization in Wireless Sensor Networks," *IEEE Signal Processing Magazine*, Vol. 22, 2005, pp. 54-69.
- [3] S. Gezici, Z. Tian, G. B. Giannakis, H. Kobayashi, A. F. Molisch, H. V. Poor, and Z. Sahinoglu, "Localization via Ultra-Wideband Radios: A Look at Positioning Aspects for Future Sensor Networks," *IEEE Signal Processing Magazine*, Vol. 22, 2005, pp. 70-84.
- [4] S. Hara, D. Zhao, K. Yanagihara, J. Taketsugu, K. Fukui, S. Fukunaga, and K. Kitayama, "Propagation Characteristics of IEEE 802.15.4 Radio Signal and Their Application for Location Estimation," *IEEE Vehicular Technology Conference*, Jun. 2005, pp. 97-101.
- [5] S. Feng and C. L. Law, "Assisted GPS and Its Impact on Navigation in Intelligent Transportation Systems," *IEEE Intelligent Transportation Systems*, 2002, pp. 926-931.
- [6] P. Farradyne, "Vehicle Infrastructure Integration (VII) - Architecture and Functional Requirements," *Federal Highway Administration (FHWA)*, Draft Version 1.0, Apr. 2005.
- [7] Y. Zhao, "Standardization of Mobile Phone Positioning for 3G Systems," *IEEE Communications Magazine*, Vol. 40, Jul. 2002, pp. 108-116.
- [8] H. Koshima and J. Hoshen, "Personal Locator Services Emerge," *IEEE Spectrum*, Vol. 37, Feb. 2000, pp. 41-48.

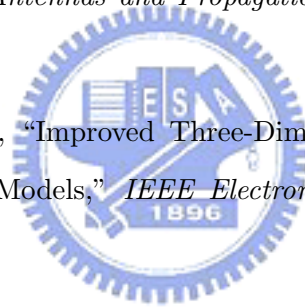
- [9] J. H. Reed, K. J. Krizman, B. D. Woerner, and T. S. Rappaport, "An Overview of the Challenges and Progress in Meeting the E-911 Requirement for Location Service," *IEEE Communication Magazine*, Vol. 36, Apr. 1998, pp. 30-37.
- [10] A. H. Sayed, A. Tarighat, and N. Khajehnouri, "Network-Based Wireless Location: Challenges Faced in Developing Techniques for Accurate Wireless Location Information," *IEEE Signal Processing Magazine*, Vol. 22, Jul. 2005, pp. 25-40.
- [11] W. H. Foy, "Position-Location Solutions by Taylor-Series Estimation," *IEEE Trans. Aerosp. Electron. Syst.*, Vol. 12, Mar. 1976, pp. 187-194.
- [12] X. Wang, Z. Wang, and B. O'Dea, "A TOA-Based Location Algorithm Reducing the Errors Due to Non-Line-of-Sight (NLOS) Propagation," *IEEE Trans. Vehicular Technology*, Vol. 52, Jan. 2003.
- [13] Y. T. Chan and K. C. Ho, "A Simple and Efficient Estimator for Hyperbolic Location," *IEEE Trans. Signal Processing*, Vol. 42, 1994, pp. 1905-1915.
- [14] L. Cong and W. Zhuang, "Hybrid TDOA/AOA Mobile User Location for Wideband CDMA Cellular Systems," *IEEE Trans. Wireless Communications*, Vol. 1, Jul. 2002, pp. 439-437.
- [15] J. Caffery Jr., "A New Approach to the Geometry of TOA Location," *IEEE Vehicular Technology Conference*, Vol. 4, Sept. 2000, pp. 1943-1949.
- [16] S. Venkatraman and J. Caffery Jr., "Hybrid TOA/AOA Techniques for Mobile Location in Non-Line-of-Sight Environments," *IEEE Wireless Communications and Networking Conference*, Vol. 1, Mar. 2004, pp. 274-278.
- [17] J. Shuhong, S. Xicai, and K. Fanru, "A Time-of Arrival Location Algorithm for Maneuvering Target on Two-dimensional Surface," *IEEE International Conference on Signal Processing*, Vol. 2, Oct. 1998, pp. 1700-1703.

- [18] M. Nájár and J. Vidal, "Kalman Tracking Based on TDOA for UMTS Mobile Location," *IEEE International Symposium on Personal, Indoor and Mobile Radio Communications*, Vol. 1, Sept. 2001, pp. B-45-49.
- [19] M. Nájár and J. Vidal, "Kalman Tracking for Mobile Location in NLOS Situations," *IEEE International Symposium on Personal, Indoor and Mobile Radio Communications Proceedings*, Vol. 3, 7-10 Sept. 2003, pp. 2203-2207.
- [20] B. L. Le, K. Ahmed, and H. Tsuji, "Mobile Location Estimator with NLOS Mitigation Using Kalman Filtering," *IEEE Wireless Communications and Networking*, Vol. 3, Mar. 2003, pp. 1969-1973.
- [21] C. L. Chen and K. F. Feng, "Hybrid Location Estimation and Tracking System for Mobile Devices," *IEEE Vehicular Technology Conference (VTC) Spring 2005*, Vol. 4, Jun. 2005, pp. 2648-2652.
- [22] N. Levanon, "Lowest GDOP in 2-D Scenarios," *IEE Proc.-Radar, Sonar Navig.*, Vol. 147, Jun. 2002, pp. 149-155.
- [23] J. Chaffee and J. Abel, "GDOP and the Cramer-Rao Bound," *PLANS*, Apr. 1994, pp. 663-668.
- [24] Y. Qi, H. Kobayashi and H. Suda, "Analysis of Wireless Geolocation in A Non-Line-of-Sight Environment," *IEEE Trans. Wireless Communications*, Vol. 5, Mar. 2006, pp. 672-681.
- [25] Y. Qi, T. Asai, H. Yoshino, and N. Nakajima, "On Geolocation in Ill-Conditioned BS-MS Layouts," *IEEE International Conference on Acoustics, Speech, and Signal Processing Proceedings*, Mar. 2005, pp. 697-700.
- [26] P. C. Chen, "A Cellular Based Mobile Location Tracking," *IEEE Vehicular Technology Conference (VTC) 1999*, Vol. 3, 16-20 May 1999, pp. 1979-1983

- [27] L. J. Greenstein, V. Erceg, Y. S. Yeh, and M. V. Clark, "A New Path-Gain/ Delay-Spread Propagation Model for Digital Cellular Channels," *IEEE Trans. on Vehicular Technology*, Vol. 46, May 1997, pp. 477-485.
- [28] C. Y. Lee, "Mobile Communications Engineering," *McGraw-Hall*, NY, 1993.
- [29] M. Scott, "GPS Accuracy for Weapon Guidance," A WSTIAC White Paper, Summer 2003. See <http://wstiac.alionscience.com/Newsletters/Vol4Num2.pdf>.
- [30] R. O. Schmidt, "Multiple Emitter Location and Signal Parameter Estimation," *IEEE Trans. Antennas and Propagation*, Vol. 34, Issue 3, Mar. 1986, pp. 276-280.
- [31] E. G. Strom, S. Parkvall, S.L. Miller, and B.E. Ottersten, "Propagation Delay Estimation of DS-CDMA Signals in A Fading Environment," *IEEE GLOBECOM.*, Nov. 1994, pp. 85-89.
- [32] P. Luukkainen, and J. Joutsensalo, "Comparison of MUSIC and Matched Filter Delay Estimators in DS-CDMA," *IEEE Personal, Indoor and Mobile Radio Communications*, Vol. 3, Sept. 1997, pp. 830-834.
- [33] E. G. Strom, S. Parkvall, S. L. Miller, and B. E. Ottersten, "Propagation Delay Estimation in Asynchronous Direct-Sequence Code-Division Multiple Access Systems," *IEEE Trans. Communications*, Vol. 44, Issue 1, Jan. 1996, pp. 84-93.
- [34] S. Gazor, S. Affes, and Y. Grenier, "Robust Adaptive Beamforming via Target Tracking," *IEEE Trans. on Signal Processing*, Vol. 44, Issue 6, Jun. 1996, pp. 1589-1593.
- [35] S. Affes, S. Gazor, and Y. Grenier, "An Algorithm for Multisource Beamforming and Multitarget Tracking," *IEEE Trans. Signal Processing*, Vol. 44, Issue 6, Jun. 1996, pp. 1512-1522.
- [36] K. Harmanci, J. Tabrikian, and J. L. Krolik, "Relationships Between Adaptive Minimum Variance Beamforming and Optimal Source Localization," *IEEE Trans. Signal Processing*, Vol. 48, Issue 1, Jan. 2000, pp. 1-12.



- [37] K. Kaemarungsi and P. Krishnamurthy, "Properties of Indoor Received Signal Strength for WLAN Location Fingerprinting," *IEEE Mobile and Ubiquitous Systems*, Aug. 2004, pp. 14-23.
- [38] J. Kwon, B. Dundar, and P. Varaiya, "Hybrid Algorithm for Indoor Positioning Using Wireless LAN," *IEEE Vehicular Technology Conference*, Vol. 7, Sept. 2004, pp.4625-4629.
- [39] K. Kaemarungsi and P. Krishnamurthy, "Modeling of Indoor Positioning Systems Based on Location Fingerprinting," *IEEE INFOCOM*, Vol. 2, Mar. 2004, pp. 1012-1022.
- [40] T. Imai and T. Fujii, "Indoor Micro Cell Area Prediction System using Ray-tracing for Mobile Communication Systems," *IEEE Personal, Indoor and Mobile Radio Communications*, Vol. 1, Oct. 1996, pp. 24-28.
- [41] K. R. Chang and H. T. Kim, "Improvement of the Computation Efficiency for A Ray-Launching Model," *IEEE Antennas and Propagation*, Vol. 145, Issue 4, Aug. 1998, pp. 303-308.
- [42] S. T. Tan and H. S. Tan, "Improved Three-Dimensional Ray Tracing Technique for Microcellular Propagation Models," *IEEE Electronics Letters*, Vol. 31, Issue 17, Aug. 1995, pp.1503-1505.
- [43] Z. Sandor, L. Nagy, Z. Szabo, and T. Csaba, "3D Ray Launch and Moment Method for Indoor Radio Propagation Purposes," *IEEE Personal, Indoor and Mobile Radio Propagation*, Vol. 1, Sept. 1997, pp.130-134.
- [44] M. Hata, "Empirical Formula for Propagation Loss in Land Mobile Radio Services," *IEEE Trans. Vehicular Tech.*, Vol. 29, Issue 3, Aug. 1980, pp. 317-325.
- [45] S. Y. Seidal and T. S. Rappaport, "Site Specific Propagation Prediction for Wireless In-Building Personal Communication System Design," *IEEE Trans. Vehicular Yechnology*, Vol. 43, Issue 4, Nov. 1994 , pp. 879-891.
- [46] W. H. Foy, "Position-Location Solutions by Taylor-Series Estimation," *IEEE Trans. Aerosp. Electron. Syst.*, Vol. 12, Mar. 1976, pp. 187-194.



- [47] P. C. Chen, “A Non-Line-of-Sight Error Mitigation Algorithm in Location Estimation,”  
*IEEE Wireless Communications Networking Conference*, Vol. 1, Sept. 1999, pp. 316-320.

